

1 **Landsat and Sentinel-derived glacial lake dataset in the**
2 **China-Pakistan Economic Corridor from 1990 to 2020**

3
4 Muchu Lesi¹, Yong Nie^{1,*}, Dan H. Shugar², Jida Wang³, Qian Deng^{1,4}, Huayong Chen¹

5 ¹Institute of Mountain Hazards and Environment, Chinese Academy of Sciences, Chengdu,
6 China.

7 ²Water, Sediment, Hazards, and Earth-surface Dynamics (waterSHED) Lab, Department of
8 Geoscience, University of Calgary, Alberta, T2N 1N4, Canada

9 ³Department of Geography and Geospatial Sciences, Kansas State University, Manhattan,
10 Kansas 66506, USA

11 ⁴University of Chinese Academy of Sciences, Beijing 100190, China

12
13
14
15 *Corresponding author, nieyong@imde.ac.cn
16
17

18 **Abstract.** The China-Pakistan Economic Corridor (CPEC) is one of ~~thea-number-of~~ flagship
19 projects of the One Belt One Road Initiative, which faces threats from mountain disasters in
20 the high altitude region, such as glacial lake outburst floods (GLOFs). An up-to-date
21 high-quality glacial lake dataset with ~~critical~~ parameters ~~likesuch as lake type, acquisition~~
22 ~~date and uncertaintyarea(e.g. lake types)~~, which is fundamental to flood risk assessments and
23 predicting glacier-lake evolutions ~~and cryosphere-hydrological interactionsechanges~~, is still
24 largely absent for the entire CPEC. This study describes a glacial lake dataset ~~in-2020~~ for
25 CPEC, ~~based on an object-oriented mapping method associated with rigorous visual~~
26 ~~inspection workflows. This dataset includes (1) a glacial lake inventory for the year 2020 at~~
27 ~~10 m resolution produced, which was produced from Sentinel opticalspectral images, and (2)~~
28 ~~multi-temporal inventories for 1990, 2000, and 2020 produced from as well as 30 m~~
29 ~~resolution Landsat imagesglacial lake inventories in 1990, 2000 and 2020 from Landsat~~
30 ~~observation at 10-30 m resolution, which was produced from both Landsat and Sentinel~~
31 ~~optical images as well as glacial lake inventories in 1990 and 2000 from Landsat observation,~~
32 ~~using an advanced object-oriented mapping method associated with rigorous visual~~
33 ~~inspection workflows.~~ The results show that Landsat derived 2234 glacial lakes in 2020,
34 covering a total area of $86.31 \pm 14.98 \text{ km}^2$ with a minimum mapping unit of 5 pixels (4500 m^2),
35 whereas Sentinel derived 7560 glacial lakes in 2020 with a total area of $103.70 \pm 8.45 \text{ km}^2$
36 with a minimum mapping unit of 5 pixels (500 m^2). The discrepancy implies that there is a
37 significant quantity of small glacier lakes not recognized in existing glacial lake inventories
38 and a more thorough inclusion of them require future efforts using higher resolution data. The
39 total number and area of glacial lakes from consistent 30 m resolution Landsat images remain
40 relatively stable despite a slight increase from 1990 to 2020. A range of critical attributes
41 have been generated in the dataset, including lake types ~~of two classification systems~~ and
42 mapping uncertainty estimated by an improved [Hanshaw's](#) equation. This comprehensive
43 glacial lake dataset has potentials to be widely applied in studies on glacial lake-related
44 hazards ~~and~~, glacier-lake interactions [and cryospheric hydrology](#), and is freely available at
45 <https://doi.org/10.12380/Glaci.msdc.000001> ([Lesi et al., 2022](#)) (~~Lesi et al., 2022~~).

46 **1 Introduction**

47 Glaciers in High-mountain Asia (HMA) play a crucial role in regulating climate, supporting
48 ecosystems, modulating the release of freshwater into rivers, and sustaining municipal water
49 supplies ([Wang et al., 2019; Viviroli et al., 2020](#)) (~~Wang et al., 2019; Viviroli et al., 2020~~),
50 agricultural irrigation, and hydropower generation ([Pritchard, 2019; Nie et al., 2021](#))-
51 (~~Pritchard, 2019; Nie et al., 2021~~). Most HMA glaciers are losing mass in the context of
52 climate change ([Brun et al., 2017; Maurer et al., 2019; Shean et al., 2020; Bhattacharya et al.,](#)
53 [2021](#)) (~~Brun et al., 2017; Shean et al., 2020; Bhattacharya et al., 2021; Maurer et al., 2019~~),
54 therefore, unsustainable glacier melt is reducing the hydrological role of glaciers and
55 impacting downstream ecosystem services, agriculture, hydropower and other socioeconomic
56 values ([Carrivick and Tweed, 2016; Nie et al., 2021](#)) (~~Nie et al., 2021~~). The present and
57 future glacier changes also alter the frequency and intensity of glacier-related hazards, such
58 as glacier lake outburst floods (GLOFs) ([Nie et al., 2018; Rounce et al., 2020; Zheng et al.,](#)

59 [2021](#)) ([Nie et al., 2018](#); [Zheng et al., 2021](#); [Rounce et al., 2020](#)), and rock and ice avalanches
60 ([Shugar et al., 2021](#)) (~~[Shugar et al., 2021](#)~~). [Global glacial lake numbers and total area both](#)
61 [increased between 1990 and 2018 in response to glacier retreat and climate change](#) ([Shugar et](#)
62 [al., 2020](#)), [which inevitably affected the risk of GLOFs.](#), ~~[altering the risk of GLOFs.](#)~~ The
63 increasing frequency of GLOFs has been observed in the Karakoram and Himalaya ([Nie et al.,](#)
64 ~~[2021](#)~~) (~~[Nie et al., 2021](#)~~), and the increasing risk of GLOFs ([Zheng et al., 2021](#)) is threatening
65 existing and planned infrastructures in the mountain ranges, such as hydropower plants,
66 railways, and highways.

67 A large number of major infrastructure construction projects for the One Belt One Road
68 Initiative (BRI) play a fundamental role in strengthening the interconnection of infrastructure
69 between countries and promoting international trade and investment ([Battamo et al., 2021](#); [Li](#)
70 [et al., 2021](#)) (~~[Battamo et al., 2021](#)~~; ~~[Li et al., 2021](#)~~). Taking the Karakoram Highway for
71 example, it is a unique land route to link China and Pakistan. The China-Pakistan Economic
72 Corridor (CPEC) is one of the BRI flagship projects, originating from Kashgar of the
73 Xinjiang Uygur Autonomous region, China and extending to Gwadar Port, Pakistan ([Ullah et](#)
74 [al., 2019](#); [Yao et al., 2020](#)) (~~[Ullah et al., 2019](#)~~; ~~[Yao et al., 2020](#)~~). The northern section of the
75 CPEC passes through Pamir, Karakoram, Hindu Kush and Himalaya mountains where
76 glacier-related hazards such as GLOFs are frequent and severe ([Hewitt, 2014](#); [Bhambri et al.,](#)
77 ~~[2019](#)~~) (~~[Hewitt, 2014](#)~~; ~~[Bhambri et al., 2019](#)~~), threatening the existing, under-construction and
78 planned infrastructure projects. Understanding the risk posed by GLOFs is a critical step to
79 disaster prevention for infrastructures across the CPEC ([Figure 1](#) ~~[Figure 1](#)~~).

80 Glacial lake inventories with a range of attributes benefit risk assessment and disaster
81 reduction related to GLOFs, and contribute to predicting glacier-lake evolution [and](#)
82 [cryosphere-hydrosphere interactions](#) under climate change ([Nie et al., 2017](#); [Brun et al., 2019](#);
83 [Maurer et al., 2019](#); [Carrivick et al., 2020](#); [Liu et al., 2020](#)) (~~[Nie et al., 2017](#)~~; ~~[Brun et al., 2019](#)~~;
84 ~~[Liu et al., 2020](#)~~; ~~[Maurer et al., 2019](#)~~). Remote sensing is the most viable way to map glacial
85 lakes and detect their spatio-temporal changes in the high-elevation zones where in situ
86 accessibility is extremely low ([Huggel et al., 2002](#); [Quincey et al., 2007](#)) (~~[Huggel et al., 2002](#)~~;
87 ~~[Quincey et al., 2007](#)~~). Studies in glacial lake inventories using satellite observations have
88 been heavily conducted at regional scales recently, such as in the Tibetan Plateau ([Zhang et](#)
89 [al., 2015](#)) (~~[Zhang et al., 2015](#)~~), the Himalaya ([Gardelle et al., 2011](#); [Nie et al., 2017](#)) (~~[Gardelle](#)~~
90 ~~[et al., 2011](#)~~; ~~[Nie et al., 2017](#)~~), the HMA ([Wang et al., 2020](#); [Chen et al., 2021](#)) (~~[Chen et al.,](#)~~
91 ~~[2021](#)~~; ~~[Wang et al., 2020](#)~~), the Tien Shan ([Wang et al., 2013](#)) (~~[Wang et al., 2013](#)~~), the Alaska
92 ([Rick et al., 2022](#)), the Greenland ([How et al., 2021](#)) and the northern Pakistan ([Ashraf et al.,](#)
93 ~~[2017](#)~~) (~~[Ashraf et al., 2017](#)~~). However, the latest glacial lake mapping in 2020 is still absent
94 along the CPEC. Among existing studies, Landsat archival images are the most widely used
95 due to their multi-decadal record of earth surface observations, reasonably high spatial
96 resolution (30 m), and publicly available distribution ([Roy et al., 2014](#)) (~~[Roy et al., 2014](#)~~).
97 Freely available Sentinel-2 satellite images show a better potential than Landsat in glacial
98 lake mapping and inventories due to their higher spatial resolution (10 m) and a global
99 coverage, but have only been available since late 2015 ([Williamson et al., 2018](#); [Paul et al.,](#)
100 ~~[2020](#)~~) (~~[Williamson et al., 2018](#)~~; ~~[Paul et al., 2020](#)~~). Glacial lake inventories using Sentinel
101 images are relatively scarce at regional scales, and studies of the latest glacial lake mapping

102 as well as comparisons of glacial lake datasets derived from Sentinel and Landsat
103 observations are still lacking.

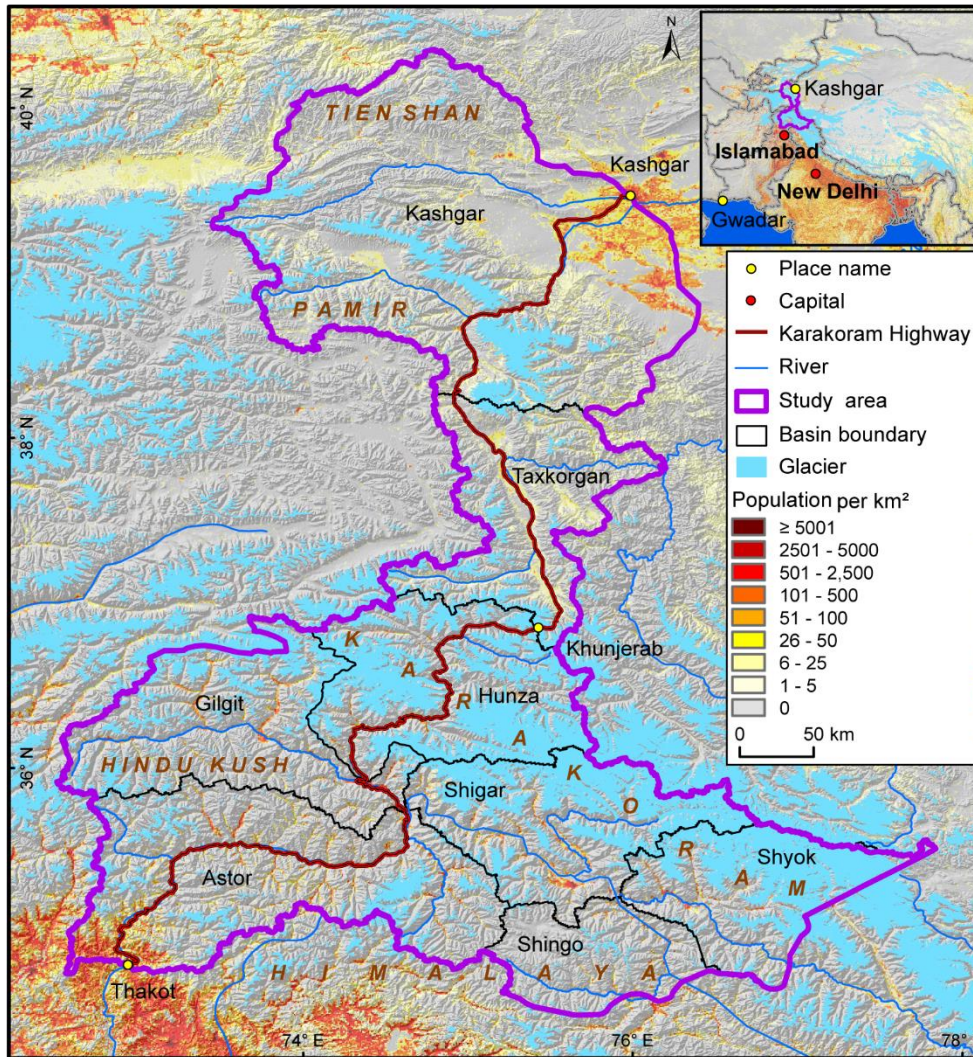
104 Discrepancies between various glacial lake inventories ([Zhang et al., 2015](#); [Shugar et al.,](#)
105 [2020](#); [Wang et al., 2020](#); [Chen et al., 2021](#); [How et al., 2021](#)) (~~[Zhang et al., 2015](#); [Shugar et](#)~~
106 ~~[al., 2020](#); [Chen et al., 2021](#); [Wang et al., 2020](#)~~) result from differences in mapping methods,
107 minimum mapping units, definition of glacial lakes, time periods, data sources and other
108 factors. For example, manual vectorization method was widely adopted at the earlier stage for
109 its high accuracy. However, it is time-consuming associated with high labor intensity and is
110 only practical at regional scales ([Zhang et al., 2015](#); [Wang et al., 2020](#)) (~~[Zhang et al., 2015](#);~~
111 ~~[Wang et al., 2020](#)~~). Automated and semi-automated lake mapping methods, such as ~~band-~~
112 ~~ratio-multi-spectral indices classification and object-oriented classification~~ ([Gardelle et al.,](#)
113 [2011](#); [Nie et al., 2017](#); [Zhang et al., 2018](#); [How et al., 2021](#)) (~~[Gardelle et al., 2011](#); [Zhang et](#)~~
114 ~~[al., 2018](#); [Nie et al., 2017](#)~~), have been developed to improve the efficiency of glacial lake
115 inventories using optical images, although ~~artificial~~ manual modification is often unavoidable
116 to assure the quality of lake data impacted by cloud cover ~~in optical images~~, mountain
117 shadows, seasonal snow cover and frozen lake surfaces ([Sheng et al., 2016](#); [Wang et al., 2017,](#)
118 [2018](#)) (~~[Sheng et al., 2016](#); [Wang et al., 2017](#); [Wang et al., 2018](#)~~). ~~S~~ Backscatter images from
119 Synthetic aAperture rRadar (SAR) backscatter classification ([Wangchuk and Bolch, 2020](#);
120 [How et al., 2021](#)) ~~was~~ ere used to remove the impact of cloud cover for lake mapping. Besides,
121 other approaches such as hydrological sink detection using DEM ([How et al., 2021](#)) ~~or~~ and
122 land surface temperature-based detection method ([Zhao et al., 2020](#)) were also used for lake
123 inventories. Different classification methods impact the results of lake mapping and
124 monitoring. data, such as sentinel-1, are also increasingly used in ice lake extraction due to
125 their undisturbed nature by clouds ([Zhang et al., 2020](#); [Wangchuk and Bolch, 2020](#)). In
126 addition, some scholars also monitor lakes based on their temperature and other
127 characteristics ([Zhao et al., 2020](#)).

128 Type-Dam type –classification of glacial lakes provides a crucial attribute for glacier-lake
129 interactions and risk assessment ([Emmer and Cuřín, 2021](#)) (~~[Emmer and Cuřín, 2021](#)~~). So far,
130 we are lacking there has not been a unified standard for the classification system of glacial
131 lakes ([Yao et al., 2018](#)) (~~[Yao et al., 2018](#)~~). Existing classification systems are mainly for their
132 respective research purposes, mainly based on the relative positions of glacial lakes and
133 glaciers, the supply conditions of glaciers, and the attributes of dams. In addition to different
134 classification standards, the same typespecies of glacial lakes may also have different names
135 given by different scholars. For example, ice-marginal ([Carrivick and Quincey, 2014](#);
136 [Carrivick et al., 2020](#)), ice-contact ([Carrivick and Tweed, 2013](#)) and proglacial ([Nie et al.,](#)
137 [2017](#)) lakes all represent glacial lakes sharing the boundary with glaciers. Glacier lakes in
138 currently available datasets have been traditionally categorized by their spatial relationship
139 with upstream glaciers ([Gardelle et al., 2011](#); [Wang et al., 2020](#); [Chen et al., 2021](#)) (~~[Gardelle](#)~~
140 ~~[et al., 2011](#); [Chen et al., 2021](#); [Wang et al., 2020](#)~~), and classification attributes considering the
141 formation mechanism and the properties of dams are rare or incomplete in the CPEC ([Yao et](#)
142 [al., 2018](#); [Li et al., 2020](#)) (~~[Li et al., 2021](#); [Yao et al., 2018](#)~~). Therefore, an up-to-date glacial
143 lake dataset with critical, quality-assured parameters (e.g. lake types) is necessary.

144 This study aims to (1) employ both Landsat 8 and Sentinel-2 images to create an up-to-date
145 glacial lake dataset in the CPEC to accurately document its detailed lake distribution in 2020;

146 (2) reveal glacial lake changes and the spatial heterogeneity across mountains and basins in
 147 the CPEC using consistent 30-m Landsat images at three time periods (1990, 2000 and 2020);
 148 and (3) share the glacial lake inventories with a range of critical attributes to benefit
 149 hazardous risk assessment of GLOFs and glacio-hydrological modeling in the HMA.

150 **2 Study area**



151
 152 **Figure 1.** Location of the study area and distribution of glaciers, mountains, basins and population.
 153

154 The study area (**Figure 1**) covers all the drainage basins along Karakoram Highway
 155 starting from Kashgar and ending at Thakot, with a total area of ~125,000 km². The upper
 156 Indus basins beyond the Pakistani-administrated border are excluded in this study due to little
 157 impact of GLOFs there on CPEC infrastructures. The entire study area is divided into eight
 158 sub-basins, covering most of the Karakoram with the highest altitude up to 8611 m, western
 159 Himalaya and Tien Shan, eastern Hindu Kush and Pamir mountains. The 9710 glaciers in the
 160 study area cover a total area of 17,447 km² and nearly 60% of glaciers are distributed in the
 161 Karakoram (5818 glaciers with a total area of 14,067.52 km²) (RGI Consortium, 2017) (RGI
 162 Consortium, 2017). Most glaciers in the western Himalaya and eastern Hindu Kush are losing
 163 mass in the context of climate change (Kääb et al., 2012; Yao et al., 2012; Brun et al., 2017;

164 [Shean et al., 2020; Hugonnet et al., 2021](#)) (~~[Kääb et al., 2012; Yao et al., 2012; Shean et al.,](#)~~
165 ~~[2020; Brun et al., 2017; Hugonnet et al., 2021](#)~~), whereas the glaciers in the eastern
166 Karakoram and Pamir have shown unusually little changes, including unchanged, retreated,
167 advanced and surged glaciers ([Hewitt, 2005; Kääb et al., 2012; Bolch et al., 2017; Brun et al.,](#)
168 [2017; Shean et al., 2020; Nie et al., 2021](#)) (~~[Nie et al., 2021; Brun et al., 2017; Shean et al.,](#)~~
169 ~~[2020; Kääb et al., 2012; Hewitt, 2005; Bolch et al., 2017](#)~~). The spatially heterogeneous
170 distribution and changes of glaciers are primarily explained as a result of differences in the
171 dominant precipitation-bearing atmospheric circulation patterns that include the winter
172 westerlies the Indian summer monsoon, their changing trends and their interactions with local
173 extreme topography ([Yao et al., 2012; Azam et al., 2021; Nie et al., 2021](#)) (~~[Azam et al., 2021;](#)~~
174 ~~[Nie et al., 2021; Yao et al., 2012](#)~~).

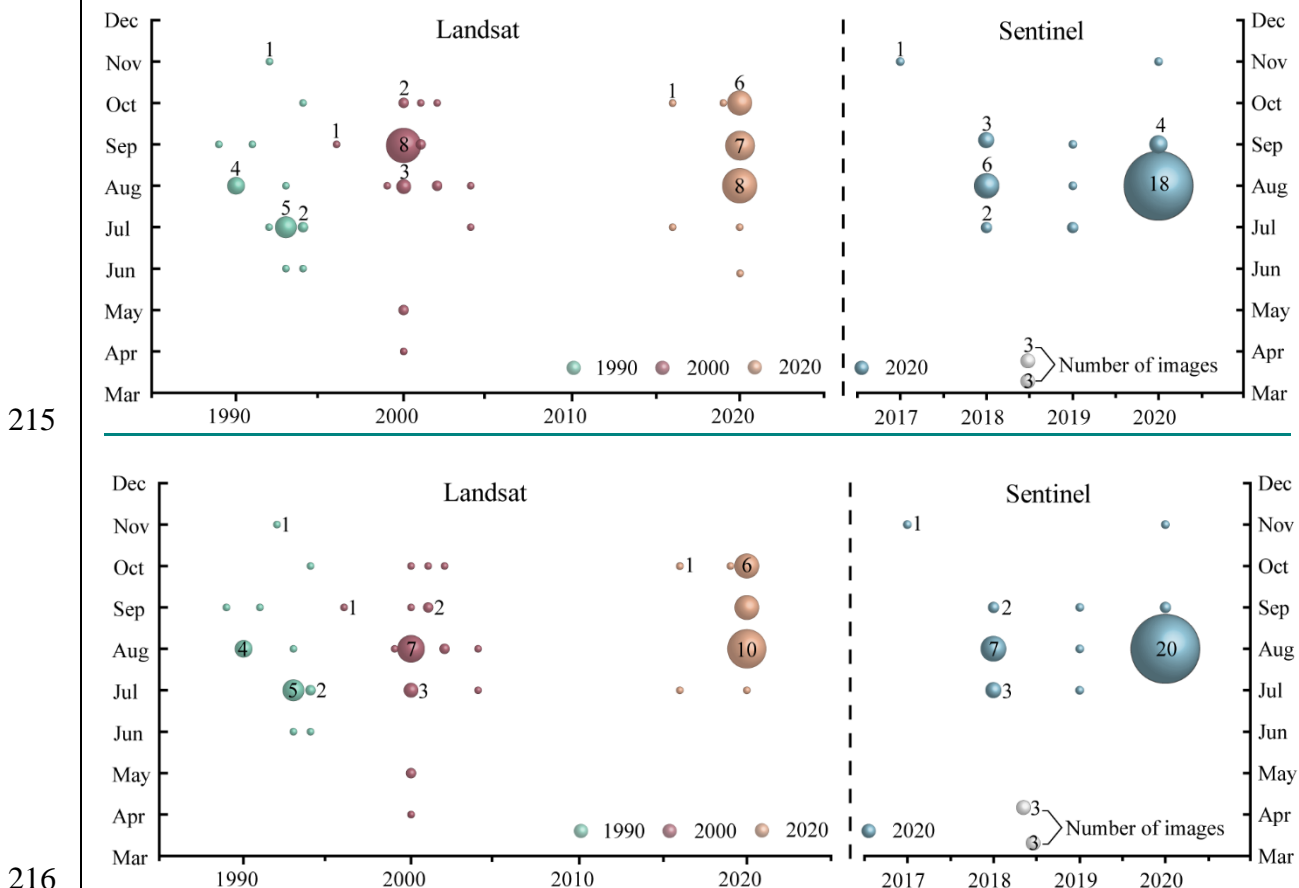
175 **3 Data sources**

176 Both Landsat and Sentinel images have been employed to map glacial lakes between 1990
177 and 2020 in the CPEC (~~[Figure 2](#)~~[Figure 2](#)). A total number of ~~98-71~~ Landsat Thematic Mapper
178 (TM), Thematic Mapper Plus (ETM+) and Landsat 8 Operational Land Imager (OLI) images
179 with a consistent spatial resolution of 30 m were downloaded from the United States
180 Geological Survey Global Visualization Viewer (GloVis, <https://glovis.usgs.gov/app/>) to be
181 used to create glacial lake inventories in 1990, 2000 and 2020. High-quality Landsat images
182 around 2010 are insufficient to cover the entire study area, so we had to give up glacial lake
183 mapping in 2010 as a result of Landsat 7's scan-line corrector errors and significant cloud
184 covers. In addition, ~~40-39~~ Sentinel-2 images were downloaded from Copernicus Open Access
185 Hub (<https://scihub.copernicus.eu/>) to produce the 10-m resolution glacial lake inventory in
186 2020.

187 Cloud and snow covers heavily affect the usability of optical satellite images ([Wulder et](#)
188 [al., 2019](#)) (~~[Wulder et al., 2019](#)~~) and their availability in the entire study area, so we took
189 advantage of the images acquired before and after each of the baseline years 1990, 2000 and
190 2020 to construct the glacial lake inventories. To minimize the impact of intra-annual changes
191 of glacial lakes, most of used images (~~8582~~% for Sentinel and ~~8275~~% for Landsat) were
192 acquired from August to October in the given baseline year with cloud coverage of <20% for
193 each image. For some specific scenes where cloud cover exceeded the threshold of 20%, we
194 selected more than one image to remedy the effect of cloud contamination ([Nie et al., 2010,](#)
195 [2017; Jiang et al., 2018](#)) (~~[Nie et al., 2010; Nie et al., 2017; Jiang et al., 2018](#)~~).

196 Other datasets used include the Randolph Glacier Inventory version 6.0 ([Pfeffer et al.,](#)
197 [2014; RGI Consortium, 2017](#)) (~~[Pfeffer et al., 2014; RGI Consortium, 2017](#)~~) and the Glacier
198 Area Mapping for Discharge from the Asian Mountains (GAMDAM) glacier inventory_
199 ([Sakai, 2019](#)) (~~[Sakai, 2019](#)~~). These two glacier datasets were used to determine glacial lake
200 ~~attributetypes, such as ice-contact, ice-dammed and unconnected-glacier-fed lakes~~. The
201 Shuttle Radar Topography Mission Digital Elevation Model (SRTM DEM) at a 1-arc second
202 (30 m) resolution ([Jarvis et al., 2008](#)) (~~[Jarvis et al., 2008](#)~~) was employed to extract the
203 altitudinal characteristics of the glacial lakes. The absolute vertical accuracy of the SRTM
204 DEM is 16 m (90%) ([Rabus et al., 2003; Farr et al., 2007](#)) (~~[Farr et al., 2007; Rabus et al.,](#)~~
205 ~~[2003](#)~~). We also applied other published glacial lake datasets for comparative analysis. They
206 include the glacial lake inventories of HMA in 1990 and 2018 downloaded from

207 <http://doi.org/10.12072/casnw.064.2019.db> (Wang et al., 2020) (Wang et al., 2020), the Third
 208 Pole region in 1990, 2000 and 2010 publicly shared at <http://en.tpdatabase.cn/> (Zhang et al.,
 209 2015) (Zhang et al., 2015), the Tibet Plateau from 2008 to 2017 accessed at
 210 <https://doi.org/10.5281/zenodo.3700282> (Chen et al., 2021) (Chen et al., 2021), and the entire
 211 world in 1990, 2000 and 2015 provided at https://nsidc.org/data/HMA_GLI/versions/1_
 212 (Shugar et al., 2020) (Shugar et al., 2020). In addition, field survey data collected between
 213 2017 and 2018 were also used to assist in lake mapping and glacial lake type classification.
 214



215
 216
 217 **Figure 22.** Acquisition years and months of Landsat and Sentinel images selected for glacial lake
 218 inventories. The bubble size indicates the available image number.

219 **4 Glacial lake inventory methods**

220 **4.1 Definition of glacial lakes**

221 We consider a glacial lake as one that formed as a result of modern or ancient glaciation.
 222 Contemporary glacial lakes are easily recognized using a combination of glacier inventories
 223 and remote sensing images. Ancient glacial lakes can be identified from periglacial
 224 geomorphological characteristics, including moraine remnants and U-shaped valleys that are
 225 discernible from satellite observations (Post and Mayo, 1971; Westoby et al., 2014; Nie et al.,
 226 2018; Mart ́n et al., 2021) (Post and Mayo, 1971; Nie et al., 2018; Mart ́n et al., 2021;
 227 Westoby et al., 2014). Landslide-dammed lakes (Chen et al., 2017) (Chen et al., 2017) in the
 228 periglacial environment were excluded in our inventories because of their irrelevance to

229 glaciation. We abandoned the definition that considers all lakes surrounding a specific
230 buffering distance of other glaciers also as glacier lakes, although this definition has been
231 widely used in previous studies assuming glacial meltwater as the main water supply (Zhang
232 et al., 2015; Wang et al., 2020) (Zhang et al., 2015; Wang et al., 2020). This is because the
233 contribution of glacial meltwater to the lake supply is arduous to be quantified without an
234 accurate modeling of the cryosphere-hydrological processes (Lutz et al., 2014) (Lutz et al.,
235 2014). All glacial lakes in the study area were mapped according to our definition without
236 any regard to buffering distance limit between lakes and of glaciers. We were able to
237 implement this definition by carefully leveraging the spectral properties of glacial lakes and
238 the periglacial geomorphological features that are often evident in remote sensing images (see
239 more in sections 4.3 and 4.4).

240 4.2 Interactive lake mapping

241 A human-interactive and semi-automated lake mapping method (Wang et al., 2014; Nie et al.,
242 2017, 2020) (Wang et al., 2014; Nie et al., 2017; Nie et al., 2020) was adopted to accurately
243 extract glacial lake extents using Landsat and Sentinel-2 images, based on the Normalized
244 Difference Water Index (NDWI) (Mcfeeters, 1996) (Mcfeeters, 1996). The NDWI uses the
245 green and near infrared bands and is calculated by the following equation:

$$246 \quad NDWI = \frac{Band_{Green} - Band_{NIR}}{Band_{Green} + Band_{NIR}} \quad (1)$$

247 where the green band and near infrared band were provided by both Landsat and Sentinel
248 multispectral images.

249 Specifically, the method calculated the NDWI histogram the method automatically
250 generated the histogram based on the pixels with of NDWI in each user-defined and
251 manually-drawn region of interest. The NDWI threshold that separates lake surface from
252 land was interactively determined by screening the NDWI histogram against the lake region
253 in the imagery (Wang et al., 2014; Nie et al., 2020) (Nie et al., 2020; Wang et al., 2012). This
254 way, the determined NDWI threshold can be well-tuned to adapt various spectral conditions
255 of the studied glacier lakes. The raster lake extents segmented by the thresholds were then
256 automatically converted to vector polygons. We first completed the glacial lake inventory in
257 2020 using this interactive mapping method, and the 2020 inventory was then used as a
258 reference to facilitate the lake mapping for other periods.

259 The minimum mapping unit (MMU) was set to 5 pixels for both Landsat (0.0045 km²) and
260 Sentinel-2 images (0.0005 km²) in this study. MMU determines the total number and area of
261 glacial lakes in the dataset, and varies in the previous studies, such as 3 pixels (Zhang et al.,
262 2015) (Zhang et al., 2015), 9 pixels (Chen et al., 2021) (Chen et al., 2021), or 55 pixels
263 (Shugar et al., 2020) (Shugar et al., 2020) for Landsat images for various objectives and
264 spatial scales. While a smaller threshold leads to a large quantity of lakes mapped, it also
265 generates larger mapping noises or uncertainties. Considering this signal-noise balance and
266 our focus on identifying prominent glacier lake dynamics in the study area, we opted to use 5
267 pixels as the minimum mapping unit MMU for both Landsat and Sentinel-2 images.




268 Several procedures were taken to assure the quality assurance and quality control for lake
269 mapping, including 1) visual inspection and modification for each lake based on Landsat,
270 Sentinel-2 and Google Earth high-resolution images overlaying preliminarily lake boundary

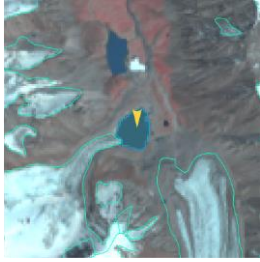
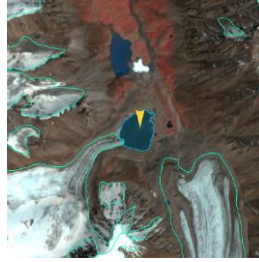

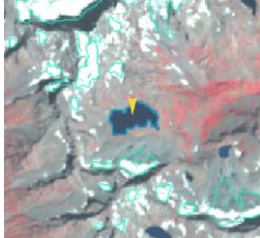
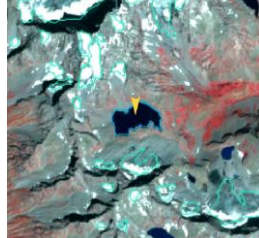




271 extraction at the given time period; 2) time series check for Landsat-derived glacial lake
 272 datasets from 1990 and 2020, and cross-check between Landsat and Sentinel-2-derived lake
 273 dataset in 2020 to reduce errors of omission and commission; 3) topological validation of
 274 glacial lake mapping, such as repeated removal, elimination of small sliver polygons; and 4)
 275 logical check for lake types between two classification systems of glacial lakes. False lake
 276 extents resulting from cloud or snow cover, lake ice, and topographic shadows (Nie et al.,
 277 2017, 2020) (Nie et al., 2020; Nie et al., 2017) and were modified using alternative images
 278 acquired in adjacent years. Those procedures were time-consuming, but helped to minimize
 279 the effect of cloud and snow covers, lake mapping errors, and to maximize the quality of the
 280 produced lake product and the derived glacial lake changes.

281 4.3 Classification of glacial lakes

282 Two glacial lake classification systems (GLCS) have been established based on relationship
 283 of interaction between glacial lakes and glaciers as well as lake formation mechanism and
 284 dam material properties. In the first GLCS (GLCS1), glacial lakes were classified into four
 285 types based on their spatial relationship to upstream glaciers: supraglacial,
 286 ~~proglacial~~ice-contact, unconnected-glacier-fed lakes, and non-glacier-fed lakes according to
 287 Gardelle et al. (2011) (2011) and Carrivick et al. (2013). Alternatively, combining the
 288 formation mechanism of glacial lakes and the properties of natural dam features, glacial lakes
 289 were classified into five categories (herein named GLCS2) modified from Yao's classification
 290 system (2018) (2018): supraglacial, end-moraine-dammed, lateral-moraine-dammed,
 291 glacial-erosion lakes and ice-blocked-dammed lakes. ~~Subglacial lakes were excluded due to~~
 292 ~~the mapping challenge~~limitation in spectral properties of optical- from spectral satellite
 293 images alone. Characterization and examples for each type are provided in ~~Table 1~~Table 1 and
 294 ~~Table 2~~Table 2. Individual glacial lakes were categorized to the specific types for each GLCS
 295 according to available glacier inventory data, geomorphological and spectral characteristics
 296 interpreted from Landsat, Sentinel and Google Earth images. The synergy of these two
 297 GLCSs is beneficial to predicting glacier-lake evolutions and providing fundamental data for
 298 glacial lake disaster risk assessment.

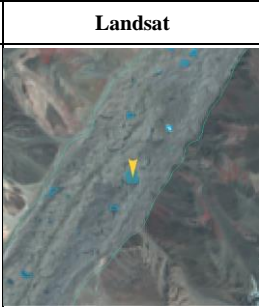

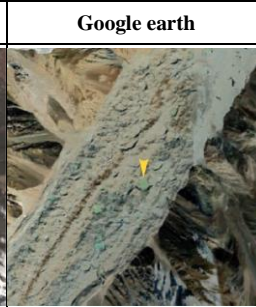
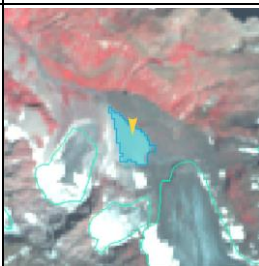
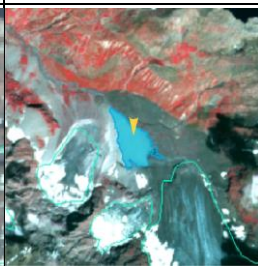


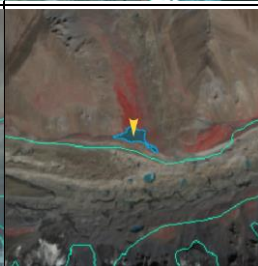


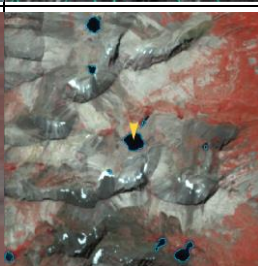

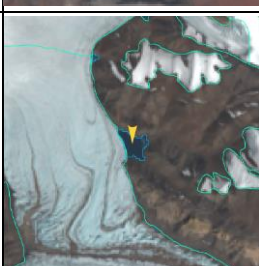
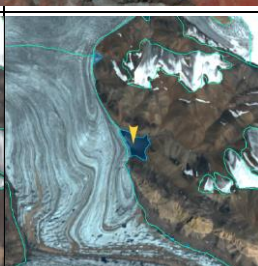
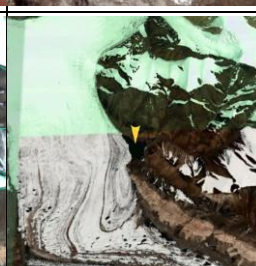
299
 300 **Table 1**. Classification system of glacial lake types according to the relationship between glacial lakes and
 301 glaciers (© Google Earth 2019).

Lake types	Characteristics	Landsat	Sentinel	Google earth
Supraglacial	Lakes formed on the surface of glaciers, generally dammed by ice and thin debris. Case location: 35°43'49.74" N 76°13'53.88" E			

<p>Proglacial/ice-contact</p>	<p>Lakes dammed by moraine, ice or bedrock, supplied by glacial meltwater and shared boundary connected with glaciers.</p> <p>Case location: 39°09'32.40" N 73°43'12.00" E</p>			
<p>Unconnected-glacier-fed</p>	<p>Lakes currently supplied by upstream glacial meltwater but disconnected with glaciers.</p> <p>Case location: 35°47'60.00" N 72°55'15.60" E</p>			
<p>Non-glacier-fed</p>	<p>Lakes formed by glaciology, dammed by moraine or bed rock, and currently not supplied by glacial meltwater.</p> <p>Case location: 34°50'39.99" N 74°48'29.31" E</p>			

303
304

Table 22. Classification system of glacial lake types according to the formation mechanism of glacial lakes and dam material properties ([© Google Earth 2019](#)).

Lake types	Characteristics	Landsat	Sentinel	Google earth
Supraglacial	Lakes formed on the surface of glaciers, generally dammed by ice and thin debris. Case location: 36°46'7.39" N 74°20'7.59" E			
End-moraine-dammed	Lakes formed behind moraines as a result of glacier retreat and downwasting. Case location: 35°42'50.40" N 73°09'57.60" E			
Lateral-moraine-dammed	Lakes formed behind lateral glacial moraine ridges and dammed by debris, different from ice-blocked-dammed glacial lake. Case location: 38°28'45.62" N 75°20'52.30" E			
Glacial-erosion	Lakes formed in depressions created by glacial over-deepening. Bedrock dam dominates, partially superimposed by top moraine in rugged terrain. Dams are unclear in the satellite images. Case location: 35°55'55.56" N 73°38'20.13" E			
Ice-blocked-dammed	Lakes formed behind glaciers, dammed by glacier ices (partially covered by debris on the top). Case location: 35°28'31.32" N 77°30'46.81" E			

305

306 4.4 Attributes of glacial lake data

307 A total of 17 attribute fields were input into our glacial lake datasets ([-Table 3Table 3](#)). They
308 include lake location (longitude and latitude), lake elevation (centroid elevation), orbital
309 number of the image source, image acquisition date, lake area, lake perimeter, lake types of
310 the two GLCSs, mapping uncertainty, and the country, sub-basin, and mountain range
311 associated with the lake. Amongst the attributes, lake location was calculated based on the
312 centroid of each glacial lake polygon associated with the DEM, N represents northing and E

313 represents easting. Orbital number of the image source was filled with the corresponding
 314 satellite image, with the codes expressed as “PxxxRxxx” or “Txxxxx”, where P and R
 315 indicate the path and row for Landsat image and T represents the tile of Sentinel image
 316 associated with 5 digits code of military grid reference system. Area and perimeter were
 317 automatically calculated based on glacial lake extents. Lake types were attributed using the
 318 characterization and interpretation marks described in Section 4.3. Mapping uncertainty was
 319 estimated using our modified equation which will be introduced in section 4.5 and
 320 [supplementary-appendix](#) tutorial. Located country, sub-basin and mountain range of each
 321 glacial lake was identified by overlapping the geographic boundaries of countries, basins and
 322 mountain ranges.

323 **Table 33.** Classification system of glacial lake types according to the formation mechanism of glacial lakes
 324 and dam material properties.

Field Name	Type	Description	Note
FID or OBJECTID	Object ID	Unique code of glacial lake	Number
Shape	Geometry	Feature type of glacial lake	Polygon
Latitude	String	Latitude of the centroid of glacial lake polygon	Degree minute second
Longitude	String	Longitude of the centroid of glacial lake polygon	Degree minute second
Elevation	Double	Altitude of the centroid of glacial lake polygon	Unit: meter above sea level
IMGSOURCE	String	Path and row numbers for Landsat image based on World Reference System 2 or Tile number for Sentinel image based on military grid reference system	PxxxRxxx or Txxxxx
ACQDATE	String	Acquisition date of source image	YYYYMMDD
GLCS1	String	The first classification system of glacial lakes based on relationship of interaction between glacial lakes and glaciers	Supraglacial, ProglacialIce-contact , Unconnected-glacier-fed, None-glacier-fed
GLCS2	String	The second classification system of glacial lakes based on lake formation mechanism and	Supraglacial, End-moraine-dammed,

Field Name	Type	Description	Note
		dam material properties	Lateral-moraine-dammed, Glacial- erosion <u>Glacial-erosion</u> and Ice-blocked <u>Ice-dammed</u>
Basin	String	Basin name where glacial lake locates in	
Mountains	String	Mountain name where glacial lake locates in	
Country	String	Country name where glacial lake locates in	
Perimeter	Double	Perimeter of glacial lake boundary	Unit: meter
Area	Double	Area of glacial lake coverage	Unit: square meter
Uncertainty	Double	Uncertainty of glacial lake mapping estimated based on modified Hanshaw's equation (2014).	Unit: square meter
Operator	String	Operator of glacial lake dataset	Muchu, Lesi
Examiner	String	Examiner of glacial lake dataset	Yong, Nie

325

326 4.5 Improved uncertainty estimating method

327 We modified Hanshaw's ~~(2014)~~(2014) equation that had been used to calculate lake-area
328 mapping uncertainty. Lake perimeter and displacement error are widely used to estimate the
329 uncertainty of glacier and lake mapping from satellite observation [\(Carrivick and Quincey,](#)
330 [2014; Hanshaw and Bookhagen, 2014; Wang et al., 2020\)](#) ~~(Wang et al., 2020; Li et al., 2020;~~
331 [Zhang et al., 2015; Gardelle et al., 2011; Carrivick and Quincey et al., 2014\)](#). Hanshaw and
332 Bookhagen ~~(2014)~~(2014) proposed an equation to calculate the error of area measurement by
333 the number of edge pixels of the lake boundary multiplied by half of a single pixel area. The
334 number of edge pixels is simply calculated by the perimeter divided by the grid size. The
335 equation is expressed as below:

$$336 \quad Error(1\sigma) = \frac{P}{G} \times 0.6872 \times \frac{G^2}{2} \quad \text{---} \quad (2)$$

$$337 \quad D = \frac{Error(1\sigma)}{A} \times 100\% \quad \text{---} \quad \text{---} \quad \text{---} \quad (3)$$

338 Where G is the cell size of the remote sensing imagery (10 m for Sentinel-2 image and 30 m
339 for Landsat image). P is the perimeter of individual glacial lake (m), and the revised
340 coefficient of 0.6872 was chosen assuming that area measurement errors follow a Gaussian
341 distribution. Relative error (D) was calculated by equation 3, in which A is the area of an
342 individual glacial lake.

343
 344
 345
 346
 347
 348

The total number of repeatedly calculated edge pixels equals the number of inner nodes. Therefore, we uncertainty estimation for lake mapping is modified as below:

349

$$Error(1\sigma) = \left(\frac{P}{G} - N_{inner}\right) \times 0.6872 \times \frac{G^2}{2} \quad (4)$$

350
 351
 352

Where N_{inner} is the number of inner nodes (inflection points) of each lake. The modified equation is also suitable for lakes with islands (as illustrated in Figure 3b).

For polygons without islands (Figure S3a), use the following equation:

353

$$N_{inner} = \left(\frac{N_{Total}-4-1}{2}\right) \quad (5)$$

354
 355
 356
 357
 358
 359
 360
 361
 362

N_{Total} is the total number of nodes, including both the outer and inner. N_{Total} were calculated by the “Field Calculator” in ArcGIS, in some cases, it is necessary to remove the redundant nodes before calculating the total number of nodes (See the Supplement for more details). An inner node is a polygon vertex where the interior angle surrounding it is greater than 180 degrees. An outer node is the opposite of the inner node, where the interior angle is less than 180 degrees. We found that the outer nodes are usually four more than the inner nodes in our glacial lake dataset. The total nodes in ArcGIS contain one overlapping node to close the polygon, meaning the endpoint is also the startpoint. This extra count was deleted in the calculation (equation 5).

363

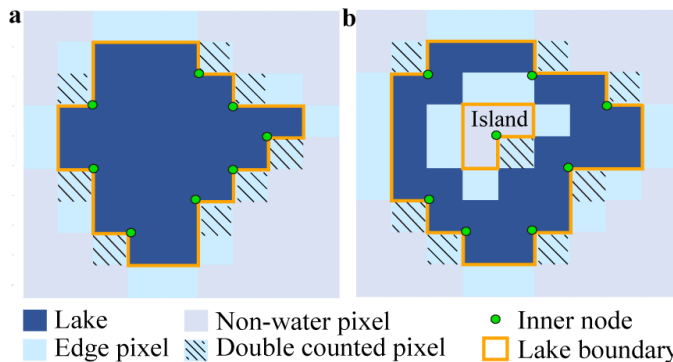
For polygons with island (Figure S3b) use the following equation:

364

$$N_{inner} = \left(\frac{N_{Total}-(N_{island}+1)\times 5}{2}\right) \quad (6)$$

365
 366
 367

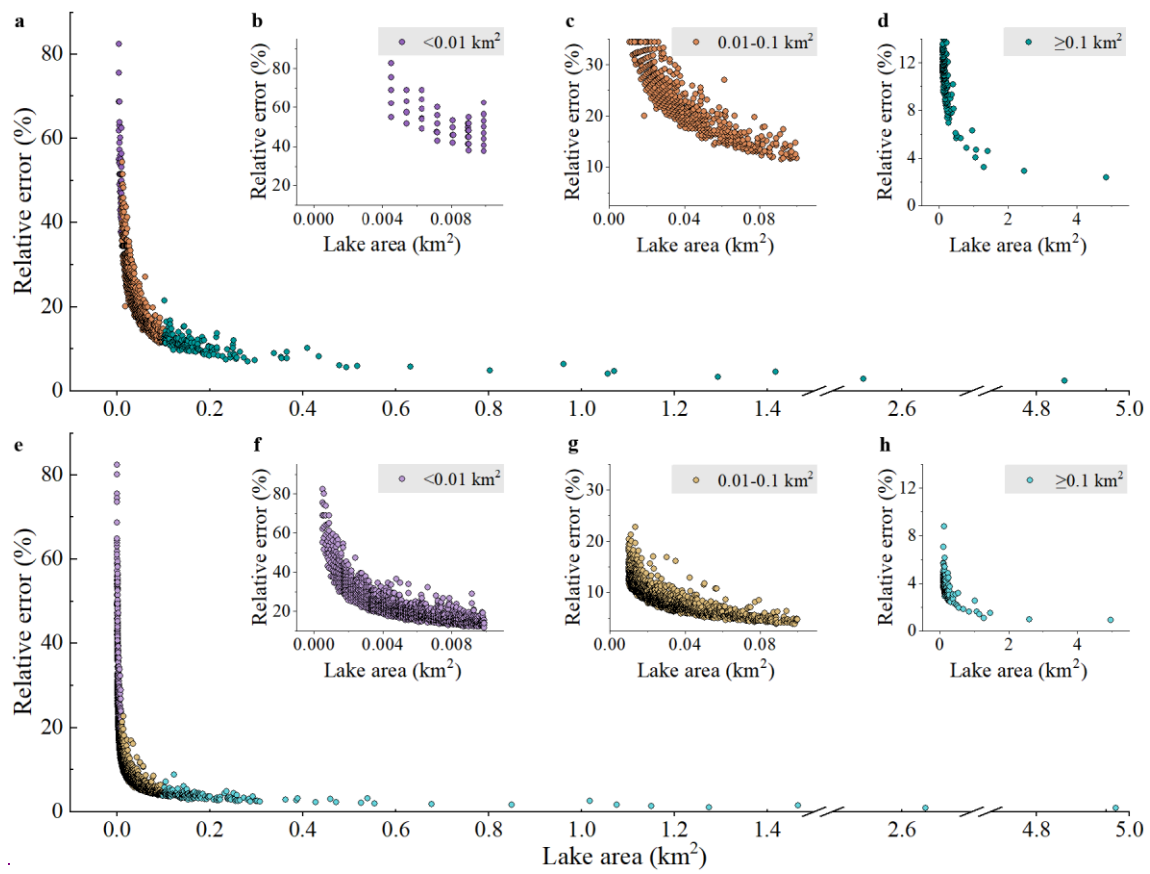
N_{island} is the number of islands within each polygon. A calculation method of N_{island} is given in the Supplement.



368
 369
 370

Figure 33. Sketch of estimating the actual edge pixels for uncertainty calculation of individual glacial lake (with and without islands).

371



372

373

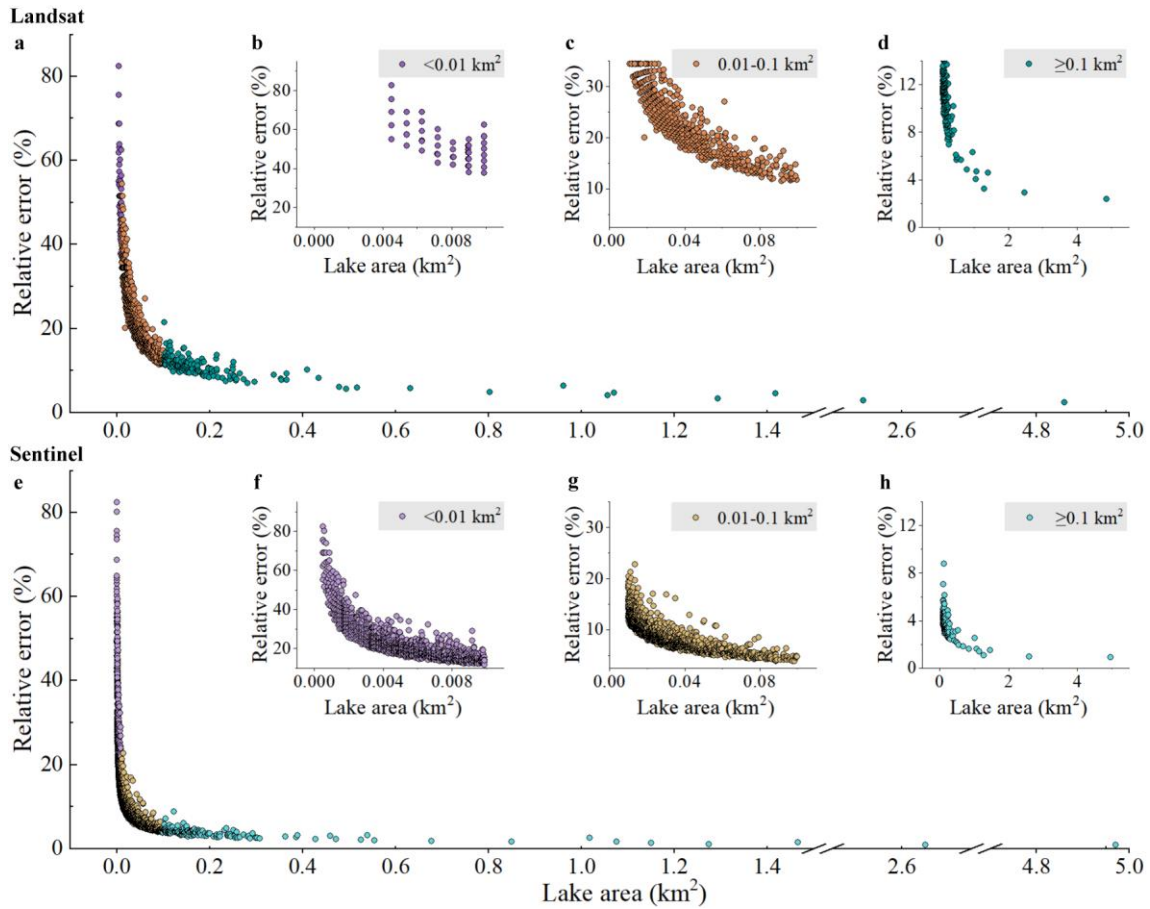


Figure 44. Relationships between individual lake size and its estimated relative error for glacial lakes of all

374 or specific size ranges in study area. Error estimation is based on the modified equation and lake data
375 extracted from Landsat (a-d) and Sentinel images (e-h).

376

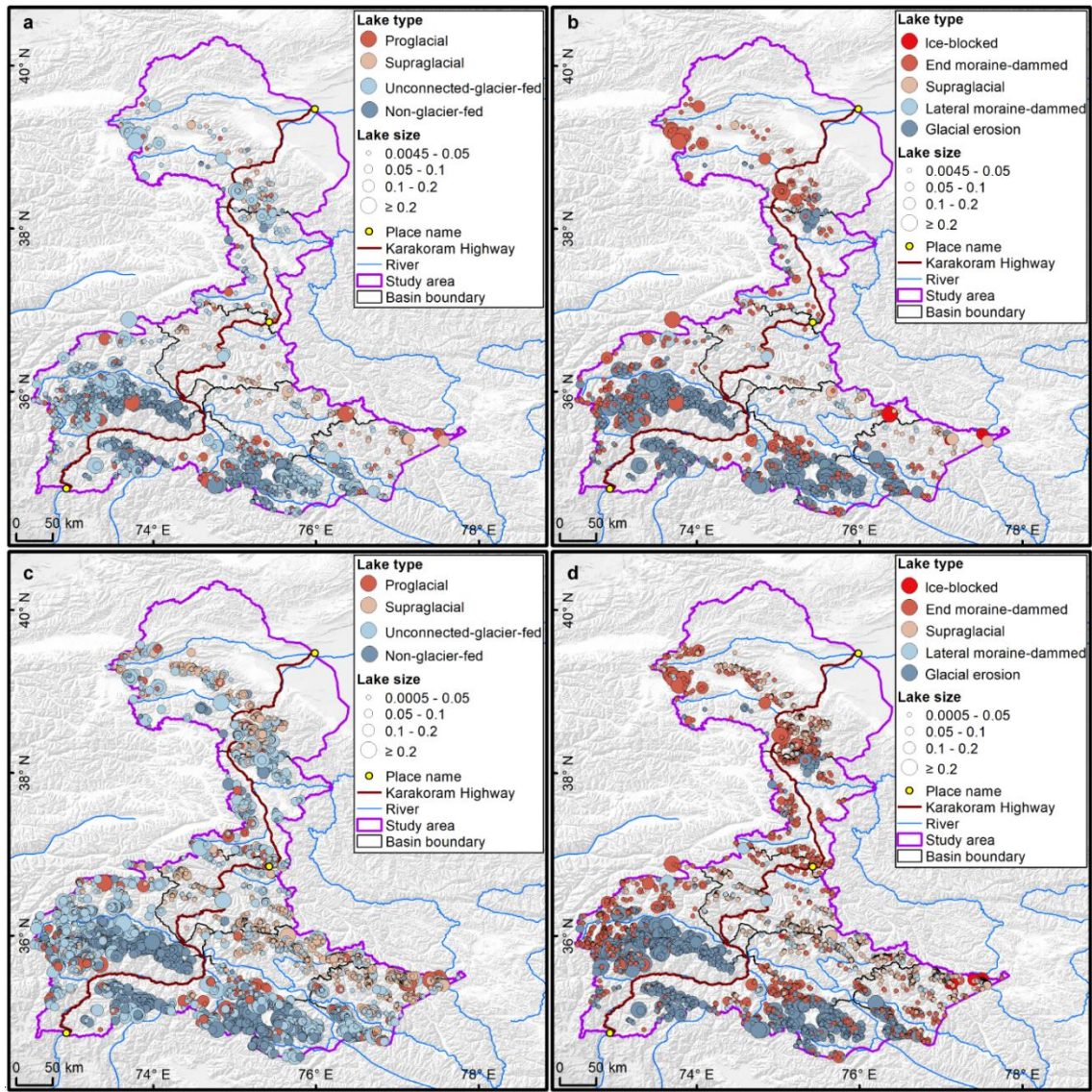
377 The uncertainty estimated from our improved equation shows that the relative error of
378 individual glacial lake decreases when lake size increases or cell size of remote sensing
379 images reduces (Lyons et al., 2013; Carrivick and Quincey, 2014) (Lyons et al., 2013;
380 Carrivick and Quincey, 2014) (Lyons et al., 2013) (Figure 4Figure-4). Total area error of
381 glacial lakes in study area is approximate $\pm 14.98 \text{ km}^2$ and $\pm 8.45 \text{ km}^2$ in 2020 for Landsat and
382 Sentinel images, respectively, and the average relative error is $\pm 17.36\%$ and $\pm 8.15\%$.
383 Generally, small lakes have greater relative errors. For example, the mean relative error is
384 35.38% for Landsat derived glacial lakes between 0.0045 and 0.1 km^2 and 10.63% for glacial
385 lakes greater than 0.1 km^2 . The mean area error of Sentinel-derived glacial lakes is almost
386 one sixth of that extracted from Landsat images for glacial lakes of all or specific size group.

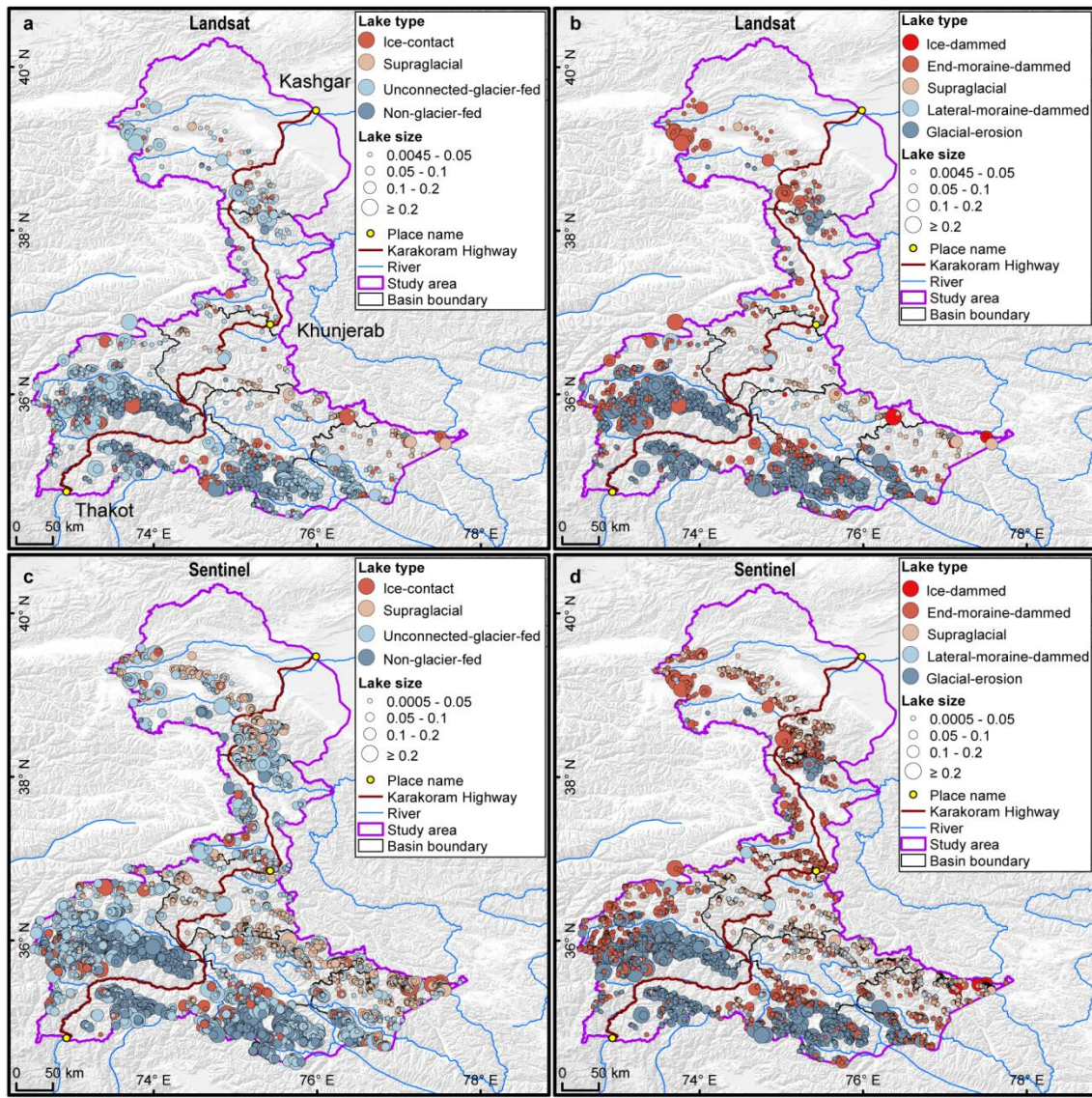
387 5 Results

388 5.1 Glacier lake distribution and changes observed from Landsat

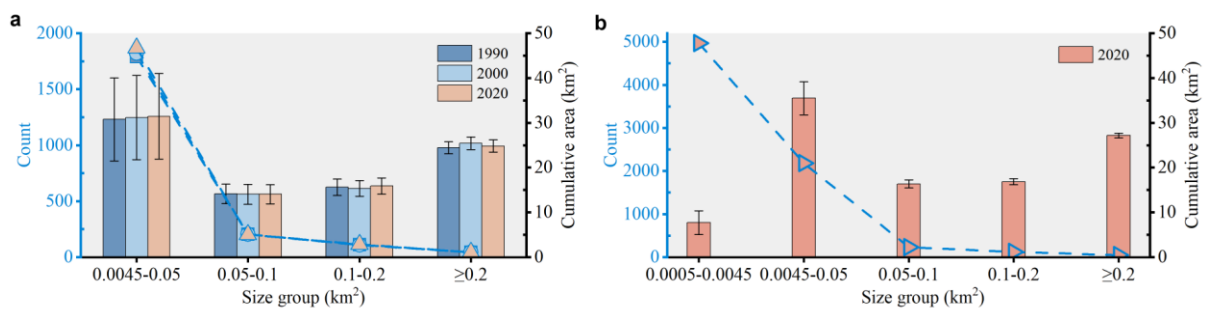
389 We mapped 2,234 glacial lakes for 2020 across the studied CPEC from Landsat-8 images,
390 with a total area of $86.31 \pm 14.98 \text{ km}^2$ (Figure 5Figure-5a and b). The majority of these glacial
391 lakes (1,870 or 83.71%) are smaller than 0.05 km^2 and contribute 36.5% of the total area. 45
392 (2.01%) of the lakes are larger than 0.2 km^2 and contribute 28.8% of the total area (Figure
393 6Figure-6). With the increase of lake size, the abundance (count) of glacial lakes consistently
394 decreases but the total lake area first reduces and then increases. Unconnected-glacier-fed
395 lakes are dominant in the first classification system, followed by non-glacier-fed lakes
396 (Figure 7Figure-7) whereas glacial-erosionglacial-erosion lakes dominate at both number
397 (1478) and area (57.02 km^2) in the second classification system (Figure 8Figure-8), followed
398 by end moraine-dammedend-moraine-dammed lakes and supraglacial lakes. Among the
399 classified lakes, 137 are proglacialice-contact lakes and cover an area of 5.56 km^2 , implying a
400 higher mean size of proglacier ice-contact lakes than supraglacial lakes.

401 Glacial lakes are spatially heterogeneous among various mountain ranges and basins in the
402 study area. Himalaya sub-region has the maximum glacier lake count and area across the
403 entire study area, followed by Hindu Kush. Supraglacial lakes are mainly distributed in the
404 Karakoram but they cover less area than those in the Pamir. Tien Shan has fewer glacial lakes.
405 Astor, Gilgit and Shingo basins have the largest percentages of glacier lakes in both number
406 and area ($>17\%$) (Figure 9Figure-9a), and each of the other basins contributes less than 10%
407 except Kashgar basin in area due to several large ancient glacial lakes. Glacial lakes of less
408 than 0.05 km^2 dominate in number within each basin and the total number decreases as lake
409 size increases. Small lakes consistently account for the maximum percentage in area except
410 Kashgar basin as a result of the disproportionally large lakes.



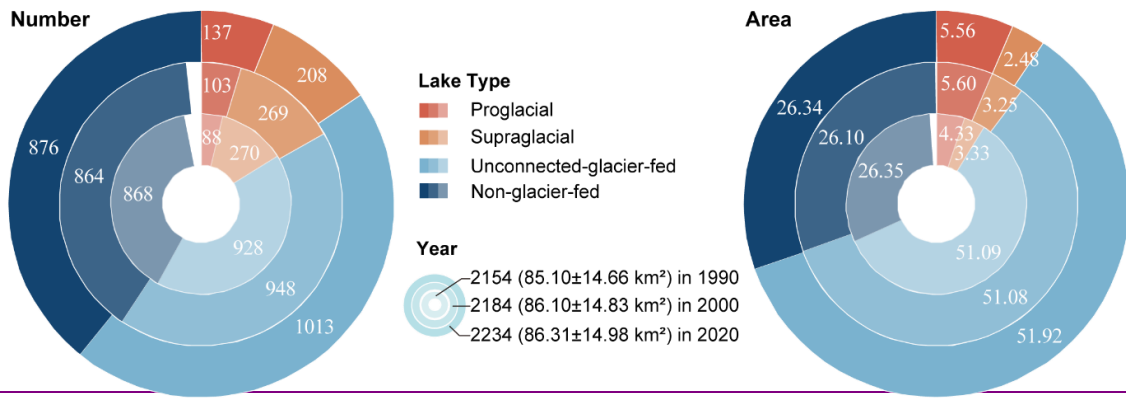


412
 413 **Figure 55.** Distribution of glacial lakes in 2020 extracted from Landsat (a, b) and Sentinel (c, d) images.
 414 Panels a and b-c are classified by GLCS1, and GLCS2 for sub-graph e-b and d.
 415

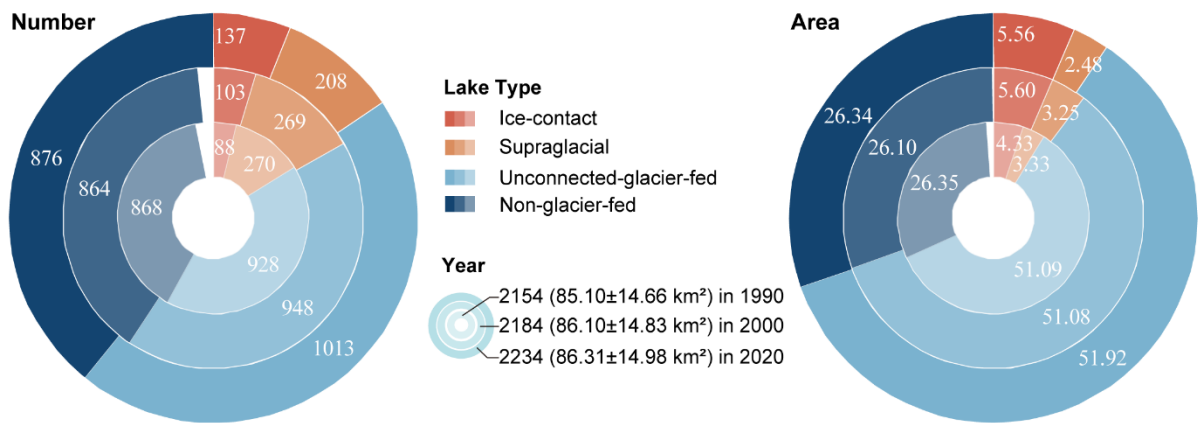


416
 417 **Figure 66.** Statistics of different sizes of glacial lakes in the study area from 1990 to 2020. Panels a and b
 418 were derived from Landsat and Sentinel images, respectively.
 419

420

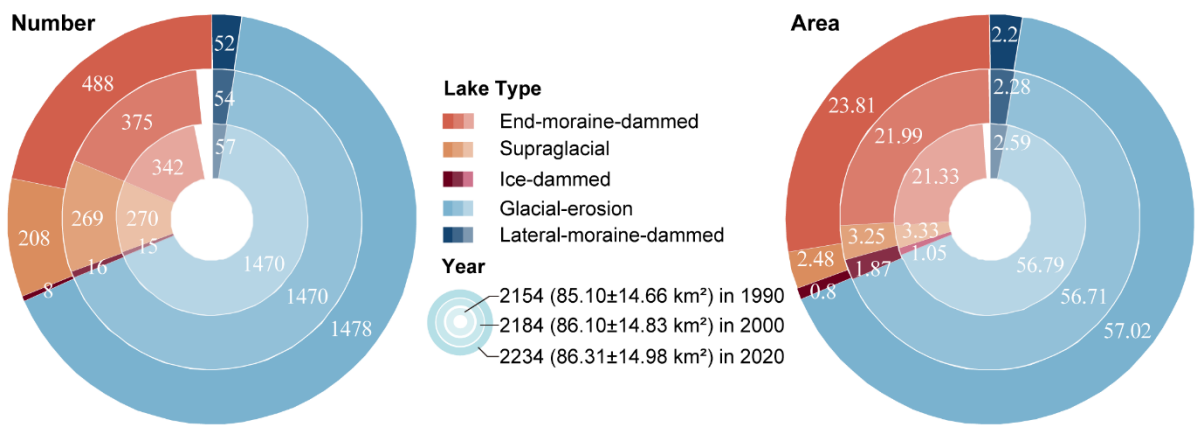


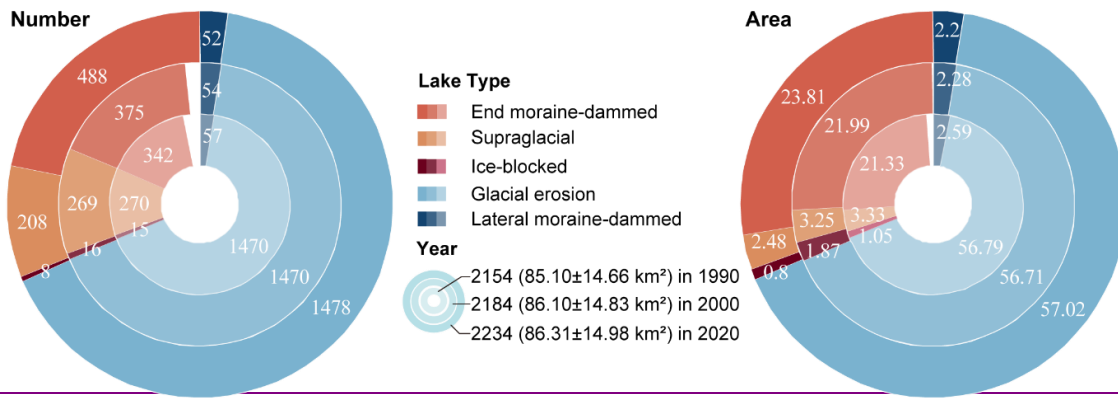
421



422 **Figure 77.** Number and area of different types of glacial lakes classified based on the condition of glacier
 423 supply in the study area. The outermost ring represents glacial lake data in 2020, middle ring for 2000 and
 424 innermost ring for 1990. Lake number and area in 2020 were selected as reference, meaning a concept of
 425 "100 %" for a complete ring. Labeled values are scaled in degrees rather the radius of rings.
 426

427





428

429

430

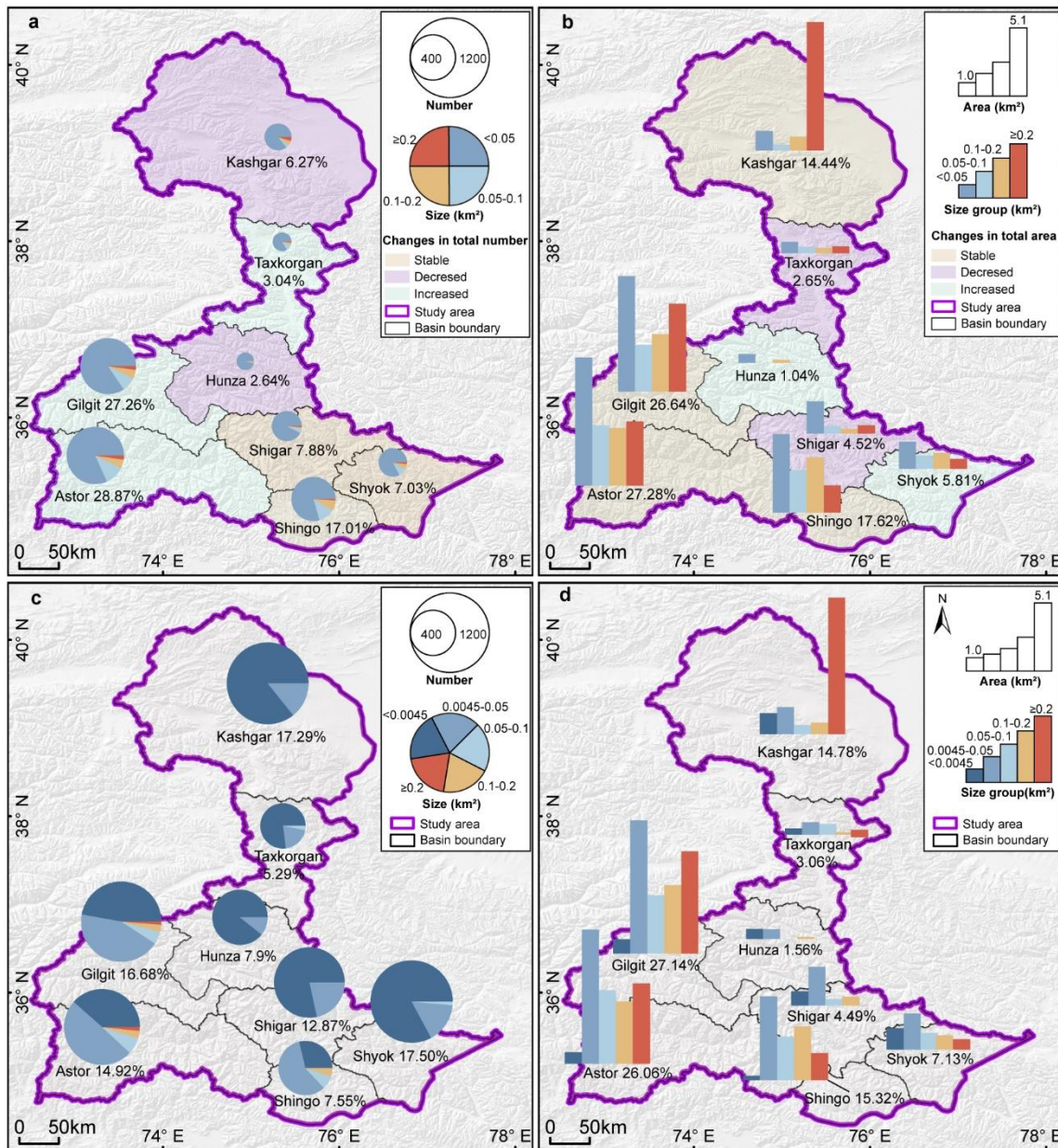
431

432

433

434

Figure 88. Number and area of different types of glacial lakes classified based on glaciation and nature of dam in the study area. The outermost ring represents glacial lake data in 2020, middle ring for 2000 and innermost ring for 1990. Lake number and area in 2020 were selected as reference, meaning a concept of "100 %" for a complete ring. Labeled values are scaled in degrees rather the radius of rings.



435
 436 **Figure 99.** Distributions and changes in count and area of glacial lakes. Percent of glacial lakes in number
 437 or area is labeled in each basin. Pie charts present the number of glacial lakes at various size groups
 438 between basins (a and c) and bar charts represent total area of glacial lakes at different size groups in each
 439 basin (b and d). The background colors represent changes in total number and area between 1990 and 2020
 440 based on Landsat derived dataset (a and b) and distribution of Sentinel derived glacial lakes in 2020 among
 441 basins are shown in sub-graphs c and d.

442
 443 The total number and area of glacial lakes in the study remain relatively stable with a slight
 444 increase between 1990 and 2020, and the changes in count and area among various types of
 445 glacial lakes vary substantially (Figure 7 and Figure 8). From 1990 to 2020,
 446 the total number of glacial lakes increased by 80 or 3.70%, while the area grew by 1.21 km²
 447 (or 1.42%) while the area grew by a less extent (1.21 km² or 1.42%). Small lakes (<math>< 0.05 \text{ km}^2</math>)
 448 continuously increased in number and area, and contributed most in the total lake expansion
 449 (Figure 6). Lakes in the size group of

450 lakes greater than 0.1 km² consistently increased.

451 In the GLCS1, unconnected-glacier-fed lakes have the largest increase in number, followed
 452 by ~~proglacial~~ice-contact and non-glacier-fed lakes, whereas supraglacial lakes decreased by
 453 62 in count. ~~Proglacial~~Ice-contact lakes expanded by 1.24 km² (equaling an increase of 26%
 454 in ~~proglacial~~ice-contact lakes), contributed one third of the total area increase. Supraglacial
 455 lakes decreased by 0.85 km² in area whereas the areas of unconnected-glacier-fed and
 456 non-glacier-fed lakes remained stable as a result of disconnections from glaciers ([Figure](#)
 457 [7Figure 7](#)).

458 In the GLCS2, ~~end moraine dammed~~end-moraine-dammed lakes increased by 2.48 km²
 459 and contributed most of the glacier lake area expansion, whereas supraglacial,
 460 ~~ice blocked~~ice-dammed and lateral--moraine-dammed lakes decreased slightly in both
 461 number and area. ~~Glacial erosion~~Glacial-erosion lakes accounted for the maximum
 462 percentage (about 66% for both count and area) in each time period and remained stable
 463 ([Figure 8Figure 8](#)).

464 Spatially, glacial lake changes in number and area vary among different mountain ranges
 465 and basins between 1990 and 2020 in the study area. Glacial lakes across the west Himalaya
 466 and Hindu Kush increased both in number and area between 1990 and 2020 whereas the total
 467 number of glacial lakes decreased in the Karakoram, Pamir and Tien Shan of study area
 468 ([Table 4Table 4](#)). The total area of glacial lakes continued to increase in the Hindu Kush, but
 469 decreased between 1990 and 2000 and increased between 2000 and 2020 in the Himalaya.
 470 The total number of glacial lakes continuously decreased in the Pamir and Tien Shan in the
 471 past three decades but increased at the first stage and decreased after in the Karakoram. The
 472 total area of glacial lakes persistently grew in the Pamir whereas fluctuated in the Tien Shan
 473 and Karakoram.

474 The total numbers of glacial lakes in Shingo, Shigar and Shyok basins were stable ([Figure](#)
 475 [9Figure 9a and b](#)); however, the areal changes were less so, including ~~being a~~ stable ~~trend~~ for
 476 Shingo, decreasing for Shigar, and increasing for Shyok. The total number of glacial lakes
 477 increased in the basins of Astor, Gilgit and Taxkorgan, whereas the total area of glacial lakes
 478 remained stable in Astor and Gilgit basins and decreased in Taxkorgan basin. The total
 479 numbers of ~~lakes in~~ Kashgar and Hunza basins decreased, whereas the total area of glacial
 480 lakes remained stable in Kashgar and increased in the Hunza basin.

481

482 **Table 44.** Distributions in count and area (km²) of glacial lakes among mountain ranges within the study area.

Source and year	Tien Shan	Karakoram	Pamir	Hindu Kush	Himalaya	Total
Landsat in 1990	10 (0.12)	370 (11.11)	178 (13.73)	780 (28.33)	816 (31.81)	2154 (85.10)
Landsat in 2000	7 (0.11)	393 (11.76)	163 (13.96)	792 (28.50)	829 (31.77)	2184 (86.10)
Landsat in 2020	5 (0.17)	334 (10.10)	182 (14.14)	835 (29.25)	878 (32.65)	2234 (86.31)
Sentinel in 2020*	11 (0.21)	479 (11.69)	262 (15.71)	880 (34.96)	959 (33.39)	2591 (95.96)

483 *Note: Glacial lake greater than 4500 m² are calculated for Sentinel-2 derived dataset in order to be in line with Landsat
 484 derived dataset.

485 5.2 Glacier lake distribution observed from Sentinel-2

486 Sentinel-derived results shows that there are 7,560 glacial lakes (103.70±8.45 km²) in 2020
 487 across the entire CPEC ([Table 5Table 5](#)) under a minimum mapping unit of 5 pixels (500 m²).

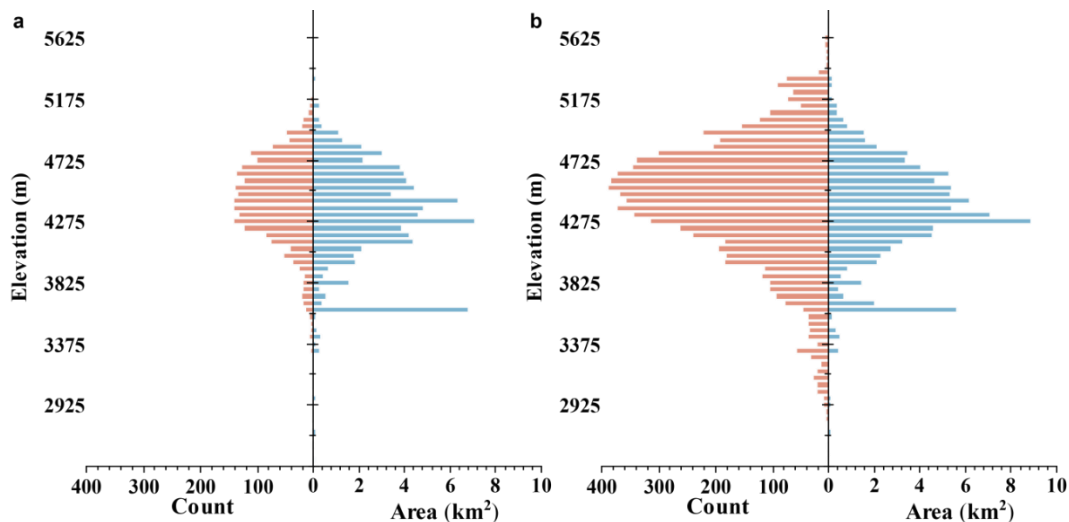
488 Similar to the pattern from Landsat mapping, the lake abundance extracted from Sentinel
 489 images is inversely related to lake size (following a typical Pareto distribution). The smallest
 490 size class (0.0005-0.0045 km²) contains the maximum lake count (4,969) but the least lake
 491 area (7.73 ±2.62 km²) ([Table 5](#)~~Table-5~~), which is not available in the Landsat-derived lake data
 492 due to a coarser spatial resolution. In each size class, there are also a higher number of larger
 493 glacial lakes from Sentinel than that from Landsat images. The discrepancy is mainly
 494 attributed to [the](#) inconsistency of [spatial resolutions and](#) image acquisition dates ~~and spatial-~~
 495 ~~resolutions~~.

496
 497 **Table 55.** Count and area of glacial lakes mapped from Sentinel and Landsat images in 2020 between
 498 various size classes

Lake size km ²	Glacial lakes from Sentinel count (km ²)	Glacial lakes from Landsat count (km ²)	Overlap % (%)
0.0005-0.0045	4969 (7.73 ±2.62)	—	—
0.0045-0.05	2182 (35.52 ±3.72)	1870 (31.47 ±9.57)	85.70 (88.60)
0.05-0.1	237 (16.37 ±0.89)	204 (14.07 ±2.18)	86.08 (85.95)
0.1-0.2	122 (16.88 ±0.68)	115 (15.91 ±1.83)	94.26 (94.25)
≥0.2	50 (27.20 ±0.54)	45 (24.86 ±1.40)	90.00 (91.40)
Total	7560 (103.70 ±8.45)	2234 (86.31 ±14.98)	—

499
 500 Compared with our Landsat-based product, glacial lakes from Sentinel-2 have similar
 501 distribution characteristics ([Figure 9](#)~~Figure-9c~~ and [d](#)) among mountain ranges, basins, types
 502 and altitudinal locations ([Figure 10](#)~~Figure-10~~); meanwhile, a larger quantity of glacier lakes, with
 503 more accurate boundaries and a greater total lake area, were generated from Sentinel-2 images. Taking
 504 altitudinal distribution for example, the number and size of glacial lakes in the study area appear follow a
 505 normal distribution against elevation for both Sentinel-2 and Landsat derived products ([Figure 10](#)~~Figure-~~
 506 ~~10~~). The elevation of all glacial lakes mapped in 2020 based on Sentinel-2 images ranged from 2500 m to
 507 5750 m (a.s.l.), with 89.58% between 3600 m and 5100 m and a mean altitude of 4421 m. The peak
 508 number appears between 4500 m and 4550 m whereas the maximum area emerges between 4250 m and
 509 4300 m. The anomalously large area between 3600 and 3650 m shows up in Fig. 10b because of several
 510 [disproportionally](#)-large lakes. Although Landsat derived lakes show a similar distribution pattern to
 511 Sentinel derived lakes, the lake count and area in each altitudinal band are greater in the Sentinel product
 512 due to the improved spatial resolution and image quality.

513



514

515 **Figure 10**. Altitudinal distribution of glacial lakes in 2020 derived from Landsat (a) and Sentinel images
 516 (b)

517

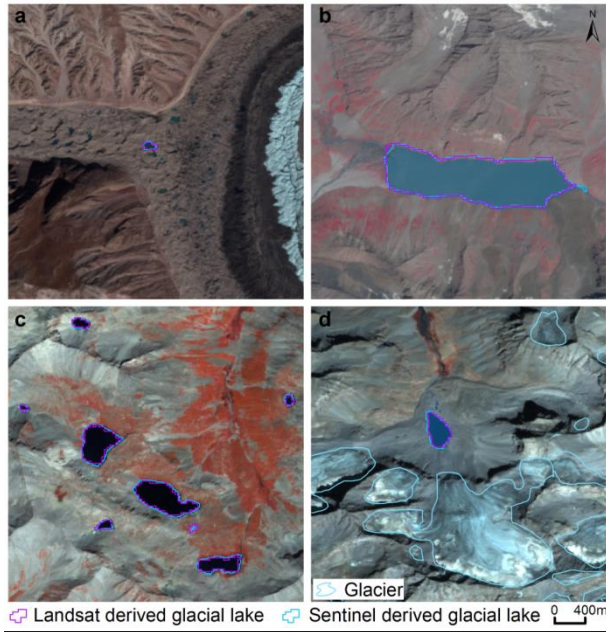
518 6 Discussions

519 6.1 Comparison of Sentinel-2 and Landsat derived products

520 Glacial lakes from Landsat and Sentinel images have a high consistency in number and area
 521 with overlap rates from 85.7% to 94.26% for all lakes greater than 0.0045 km² approximately
 522 (Table 5), implying a good potential for coordinated utility with Landsat archived
 523 observation (Figure 11). Lake extents extracted from Landsat and Sentinel images
 524 match well for various types and sizes (Table 4). The best consistency rate reaches 94%
 525 for the glacial lakes between 0.1 km² and 0.2 km². The difference in area of glacial lakes
 526 extracted from Landsat and Sentinel images generally lies within the uncertainty ranges.

527 The high consistency of Sentinel-2 and Landsat derived glacial lake products in 2020
 528 assuresimproves the value of our lake dataset. Taking the usage in assessingthe assessment
 529 of GLOFs as an example, we set 0.05 km² as the area threshold to select object lakes,
 530 including ice-contact lakes and ice-dammed lakes that are the most active lakes and source
 531 lakes of GLOFs in the CPEC (Nie et al., 2021). A total of 24 and 29 ice-contact lakes were
 532 selected from Landsat and Sentinel-derived productdataset, respectively. Among them, there
 533 were 4 ice-dammed lakes from the Landsat-derived productdataset, and 5 from the
 534 Sentinel-derived productdataset. All-these selected lakes can be used for GLOFs hazard
 535 evaluation. Because of the high consistency between our Landsat and Sentinel-based
 536 mappings, Users may have the flexibility are-able-to customizeset their-own-the lake size
 537 criteria to facilitate their specific purposesto-select-object-lakes-and-benefit-a-lot-from-our-
 538 dataset.

539



540

541 **Figure 11.** High consistency of lake extents extracted from Landsat and Sentinel images. Lake types
 542 shown include supraglacial (a), glacier-fed moraine-dammed (b), unconnected ~~glacial-~~
 543 ~~erosion~~glacial-erosion lake without glacier melt supply (c) and glacier-fed moraine-dammed (d).

544

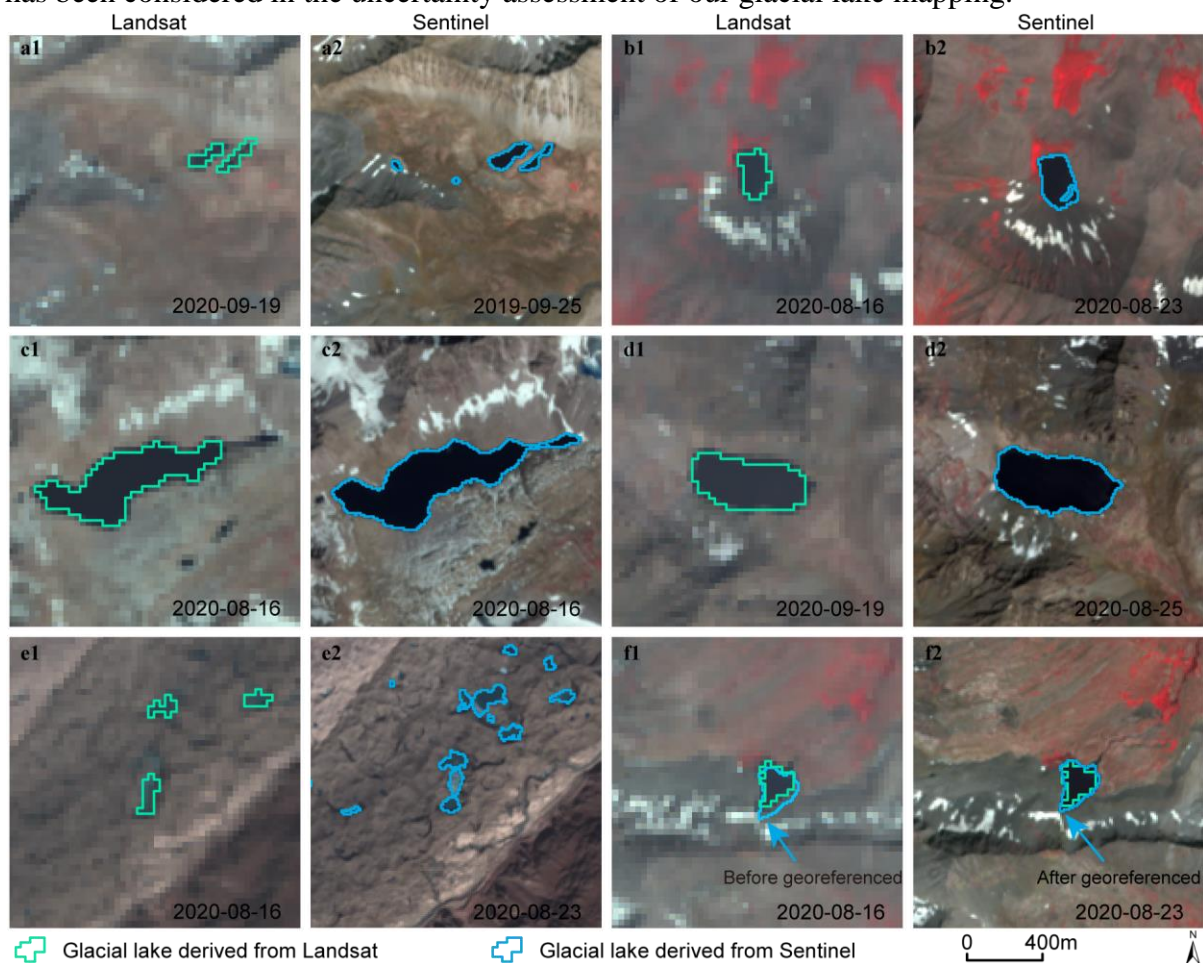
545 Spatial resolution of satellite images plays a primary role in the discrepancies in count and
 546 area of glacial lakes extracted from Landsat (30 m) and Sentinel (10 m) observations. Due to
 547 a finer spatial resolution, Sentinel images can extract more glacial lakes and more accurate
 548 extents than those from Landsat images. We set the same 5 pixels as the minimum mapping
 549 unit for both Landsat and Sentinel images, which corresponds to a minimum area of 0.0045
 550 km² and 0.0005 km², respectively. The minimum mapping area results in generating nearly
 551 5000 more lakes from Sentinel images than from Landsat images, causing the greatest
 552 discrepancy in number of the two glacial lake products (Table 5Table-5), such as Figure
 553 ~~12Figure-12a~~. ~~Small lakes, such as for example supraglacial lakes play an important role in~~
 554 ~~understanding glacier meltwater runoff surface melting, and supraglacial drainage systems-~~
 555 ~~glacier and lake evolutions, and cryospheric hydrology~~ (Liu and Mayer, 2015; Miles et al.,
 556 2018). Our dataset can be used not only for GLOFs evaluation, but also for glacial lake
 557 evolution simulation and glacio-hydrological prediction. Meanwhile, Sentinel images are able
 558 to depict boundaries of glacial lake with a lower uncertainty (Figure 12Figure-12b-d). For
 559 example, some small islands and narrow channels (Figure 12Figure-12b and c) were mapped
 560 from Sentinel imagery that ~~are~~were unable to be detected in Landsat imagery.

561

562 Different acquisition dates between Sentinel and Landsat images also contribute to the
 563 discrepancy of those two glacial lake datasets. Acquiring same-day images from the two
 564 sensors were not always possible due to the impacts of cloud contaminations, topographic
 565 shadows, snow cover and revisit periods (Williamson et al., 2018; Paul et al., 2020)-
 566 (Williamson et al., 2018; Paul et al., 2020). Glacial lakes are changing temporally in the
 567 context of climate and glacier changes, taking supraglacial lakes for example that evolve
 568 dramatically in a short period (Figure 12Figure-12e). Despite our efforts of leveraging all
 available high-quality images, the overlap of acquisition dates between Landsat and Sentinel

569 images for the same location is relatively low ([only 7 scenes of Sentinel images or 112 glacial](#)
 570 [lakes in 2020](#)) in this study area, and the consequential temporal gaps led to a difference in
 571 the number and area of the derived glacial lakes.

572 Displacement between images also resulted in a certain degree of discrepancy between
 573 Landsat and Sentinel derived glacial lakes. All images used in this study have been
 574 orthorectified [before download](#), but we still find that [a few one](#) Sentinel images [were was](#) not
 575 well matched with Landsat images, leading to the discrepancy between the two glacial lake
 576 datasets ([Figure 12](#)~~Figure 12~~f). We manually georeferenced the shifted images to minimize
 577 the difference between Sentinel and Landsat derived glacial lakes ([Figure 12](#)~~Figure 12~~f).
 578 Original geo-referencing accuracy is [approximately](#)~~approximate~~ half of one pixel for Landsat
 579 and Sentinel image, and this displacement likely contributes a minor error to glacial lake
 580 changes at various time periods. Although we could not eliminate this intrinsic error, the error
 581 has been considered in the uncertainty assessment of our glacial lake mapping.



582 **Figure 12**. Discrepancy of lake extents extracted from Landsat and Sentinel images.
 583
 584

585 6.2 Comparison with other datasets

586 Glacial lake datasets play a fundamental role in GLOF risk evaluation, glacier change
 587 prediction, and water resource availability. An increasing number of glacial lake datasets
 588 have been released over the past years, and most of them were produced from long-term
 589 Landsat archives. [Glacial-Regional glacial](#) lake datasets using Sentinel images are ~~so~~ scarce.

590 [Lack of Sentinel-derived glacial lake dataset in the study area makes it impossible to compare](#)
 591 ~~that we are unable to compare our product with other existing ones in the study area.~~ Here we
 592 selected four available glacial lake datasets to compare with our Landsat-derived dataset.

593 Our study provides the latest glacial lake dataset (in 2020) and the most long-term Landsat
 594 observation (1990 to 2020) for this study, with a range of critical attributes including two
 595 types of classification systems. Within the same study area, our 2020 glacial lakes appear to
 596 be closest to the 2018 dataset produced by Wang et al [\(2020\)-\(2020\)](#), with the highest overlap
 597 of greater than 74% in both number and area ([Table 6Table-6](#)). In Wang et al. [\(2020\)-\(2020\)](#) ,
 598 the minimum mapping unit is 6 pixels so their dataset has a smaller lake quantity. However,
 599 their dataset contains all lakes within 10 km of glacier boundaries, including many large
 600 landslide-dammed lakes that are excluded in our glacial lake mapping. As a result, their total
 601 glacier lake area is greater than ours. The overlapping rates between Wang’s glacial lakes_
 602 [\(2020\)-\(2020\)](#) in 1990 and ours are more than 69% in both number and area. However, their
 603 results show a distinct increase of glacial lakes in number and area between 1990 and 2018_
 604 [\(Wang et al., 2020\)-\(Wang et al., 2020\)](#) whereas our data show a more stable change between
 605 1990 and 2020. One possible reason is that manually delineating glacial lakes twice by
 606 different operators during Wang’s lake mapping [\(2020\)-\(2020\)](#) exacerbates the errors of
 607 mapping. Another reason is that their data contains landslide-dammed lakes that fluctuate
 608 greatly with time and expanded recently. One example is the Attabad Lake (Located at
 609 36 °18'22.33"N, 74 °49'34.36"E).

610

611 **Table 66.** Comparison of different glacial lake datasets sourced from Landsat images in the study area.

Acquisition year (period)	Method	MMU m ² (pixels)	Count (km ²)	Overlap % (%)	Reference
1990 (1988-1993)	Manual	5400 (6)	1720 (89.68±13.69)	69.17 (76.33)	Wang et al., 2020
1990 (1990-1999)	Automated	50000 (55)	145 (20.28)	6.27 (21.66)	Shugar et al., 2020
1990 (1989-1992)	Manual	2700 (3)	622 (51.93±10.15)	27.72 (39.94)	Zhang et al., 2015
1990 (1989-1994)	Automated & Manual	4500 (5)	2154 (85.10±14.66)	—	<i>This study</i>
2000 (1999-2001)	Manual	2700 (3)	724 (61.41±11.91)	31.91 (46.97)	Zhang et al., 2015
2000 (2000-2004)	Automated	50000 (55)	155 (22.35)	6.78 (23.72)	Shugar et al., 2020
2008	Automated & Manual	8100 (9)	1067 (65.45)	44.14 (53.58)	Chen et al., 2021
2000 (1996-2004)	Automated & Manual	4500 (5)	2184 (86.10±14.83)	—	<i>This study</i>
2018 (2017-2018)	Manual	5400 (6)	1956 (102.46±15.48)	74.57 (85.63)	Wang et al., 2020
2015 (2015-2018)	Automated	50000 (55)	148 (21.45)	6.27 (22.97)	Shugar et al., 2020
2017	Automated & Manual	8100 (9)	1063 (63.23)	45.21 (57.78)	Chen et al., 2021
2020 (2016-2020)	Automated & Manual	4500 (5)	2234 (86.31±14.98)	—	<i>This study</i>

612 Note: MMU represents minimum mapping units.

613

614 The second highest overlapping rate is approximate 55% in area with Chen’s data in 2008
 615 and 2017 [\(Chen et al., 2021\)-\(Chen et al., 2021\)](#). However, the overlapping rate in number is
 616 nearly 45% due to their larger minimum mapping unit (9 pixels). Similarly, a minimum
 617 mapping unit of 55 pixels (50000 m²) in Shugar et al.’s, dataset [\(2020\)-\(2020\)](#) led to the
 618 lowest overlap with less than 24% in area. [The dataset from Zhang et al. \(2015\)](#)
 619 ~~[\(2015\) ...Zhang’s dataset](#)~~ shows fewer glacial lakes in 1990 and 2000 even with a smaller

620 minimum mapping unit of 3 pixels (~~Zhang et al., 2015~~). By inspecting their dataset, we
621 attributed this anomalous discrepancy to a range of glacial lakes that were ~~missinged due to~~
622 lack of thorough cross-check quality assurance and the limit of a 10-km buffer zone from
623 glaciers during their manual delineation ~~as a result of insufficient high quality images in the~~
624 ~~earlier Landsat era~~. Our Landsat derived glacial lake dataset has been visually cross-checked
625 over three time periods after the step of object-based automated lake mapping, and also been
626 visually validated by Sentinel-2 derived glacial lakes. Through this series of quality assurance,
627 we aim at delivering one of the most reliable multi-decadal glacial lake products for this
628 study area.

629 Other factors, such as minimum mapping units, definition of glacial lakes and study areas,
630 image quality and acquisition dates, mapping methods and quality assurance workflow, might
631 also lead to the discrepancies between the glacial lake datasets. Despite such discrepancies,
632 an increasing number of publically-shared datasets benefit potential users to select the most
633 suitable one for their objectives. Herein, we provide an up-to-date glacial lake dataset derived
634 from both Landsat and Sentinel observations, which further increased the
635 availabilityoptionality of glacial lake datasets promoted the capacity offor GLOFs risk
636 assessment, ~~and~~ predicting glacier evolutions (Carrivick et al., 2020) cryosphere-hydrological
637 changes in the context of climate change.

638 6.3 Limitation and updating plan

639 We would like to acknowledge several limitations of our glacier lake dataset, largely due the
640 availability of high quality satellite images in the study area and inadequate field survey data
641 (Wang et al., 2020; Chen et al., 2021) (~~Wang et al., 2020; Chen et al., 2021~~). First, it is
642 unlikely to collect enough good-quality images within one calendar year for the entire study
643 area due to high possibility of cloud or snow covers. Even though the capacity of repeat
644 observations ~~Even though an capacity of repetitive observations~~ for Landsat-8 OLI and
645 Sentinel-2 increased (Roy et al., 2014; Williamson et al., 2018; Wulder et al., 2019; Paul et
646 al., 2020) (~~Williamson et al., 2018; Paul et al., 2020; Roy et al., 2014; Wulder et al., 2019~~),
647 the 2020 glacial lake dataset has to employ images acquired in other years besides 2020.
648 Most images used from Landsat and Sentinel platforms were imaged in autumn, and some
649 images taken between April and July and in November also were employed. Distribution and
650 changes in glacial lakes primarily represent the characteristics between August and October.
651 Glacial lakes evolve with time and space (Nie et al., 2017) (~~Nie et al., 2017~~), and subtle inter-
652 and intra-annual changes (Liu et al., 2020) (~~Liu et al., 2020~~) for each time periodin glacial-
653 lake dataset of each time period were ignored. Second, field investigation data are limited due
654 to low accessibility of high mountain environment in the study area, which restrained the
655 accuracy in classifying the glacial lake types. Although very high-resolution Google Earth
656 images were utilized to assist in lake type interpretation, occasional misclassification was
657 inevitable. We implemented two types of classification systems based on a careful utilization
658 of glacier data, DEM, geomorphological features and expert knowledge. However, the lack of
659 in situ survey prohibited a thorough validation of the glacial lake types.

660 7 Data availability

661 Our glacial lake dataset extracted from Sentinel-2 images in 2020 and Landsat observation
662 between 1990 and 2020 are available online via the Mountain Science Data Center, the
663 Institute of Mountain Hazards and Environment, the Chinese Academy of Sciences at
664 <https://doi.org/10.12380/Glaci.msdc.000001> (Lesi et al., 2022)–(Lesi et al., 2022). The glacial
665 lake dataset is provided in both ESRI shapefile format (total size of 22.6 MB) and the
666 Geopackage format (version 1.2.1) with a total size of 9.2MB, which can be opened and
667 further processed by open-source geographic information system software such as QGIS. The
668 glacial lake dataset will be updated using newly collected Landsat and Sentinel images at a
669 five-year interval or modified according to user feedbacks. The updated glacial lake dataset
670 will continue to be released freely and publicly on the Mountain Science Data Center sharing
671 platform.

672 8 Conclusions

673 Glacial lake inventories of the entire China-Pakistan Economic Corridor in 2020 were
674 completed based on Landsat and Sentinel-2 images using a human-interactive and
675 semi-automated mapping method. Both Landsat and Sentinel derived glacial lake datasets
676 show similar characteristics in spatial distribution and in the statistics of count and area. By
677 contrast, glacial lake dataset derived from Sentinel-2 images with a spatial resolution of 10 m
678 has a lower mapping error and more accurate lake boundary than those from 30 m spatial
679 resolution Landsat images whereas Landsat imagery is more suitable to analyze
680 [spatial-temporal changes at a longer time scale](#)~~spatial-temporal changes at longer time scale~~
681 due to its long-term archived ~~observations~~[observation](#) at a consistent spatial resolution of 30
682 m ~~starting~~[started](#) from around 1990.

683 Glacial lakes in the study area remain relatively stable with a slight increase in number and
684 area between 1990 and 2020 according to Landsat observations. Our dataset reveals that 2154
685 glacial lakes in 1990 covering $85.1 \pm 14.66\text{km}^2$ increased to 2234 lakes with a total area of
686 $86.31 \pm 14.98\text{km}^2$. The same mapping method and rigorous workflow of quality assurance
687 and quality control used in this study reduced the error in multi-temporal changes of glacial
688 lakes.

689 The Hanshaw's error estimation method for automated lake mapping was improved by
690 removing repeatedly calculated edge pixels that vary with lake shape. Therefore, the newly
691 proposed method reduces the estimated value of uncertainty from satellite observations.

692 Our glacial lake dataset contains a range of critical parameters that maximize their
693 potential utility for GLOFs risk evaluation, [cryosphere-hydrological](#) and glacier-lake
694 evolution projection. The dual classification systems of glacial lake types were developed and
695 are very likely to attract broader researchers and scientists to use our datasets. In comparison
696 with other existing glacial lake datasets, our products were created through a thorough
697 consideration of lake types, cross checks and rigorous quality assurance, and will be updated
698 and released continuously in the data center of mountain science. As such, we expect that our
699 glacial lake dataset will have significant [value to](#) ~~values for~~ cryospheric-hydrology research,
700 [the](#) assessment of glacier-related hazards and engineering project construction in the CPEC.

701
702 **Supplement.** The supplement related to this article is available online.

703
704 **Author contributions.** ML and YN conceived the study, ML, YN and XD performed data
705 processing and analysis of the glacial lake inventory data, JW contributed to tool development
706 and mapping methods, ML and YN wrote the manuscript. All authors reviewed and edited the
707 manuscript before submission.

708
709 **Competing interests.** The authors declare no conflict of interest.

710
711 **Acknowledgements.**
712 This study was supported by the National Natural Science Foundation of China (Grant Nos.
713 42171086, 41971153), the International Science & Technology Cooperation Program of
714 China (No. 2018YFE0100100), the Chinese Academy of Sciences “Light of West China” and
715 Natural Sciences and Engineering Research Council of Canada (Grant No. DG-2020-04207).

716
717
718
719
720 **References**

- 721 [Ashraf, A., Naz, R., Iqbal, M.B.: Altitudinal dynamics of glacial lakes under changing climate in the Hindu](#)
722 [Kush, Karakoram, and Himalaya ranges. *Geomorphology*, 283: 72-79,](#)
723 <https://doi.org/10.1016/j.geomorph.2017.01.033>, 2017.
724 [Azam, M.F., Kargel, J.S., Shea, J.M., Nepal, S., Haritashya, U.K., Srivastava, S., Maussion, F., Qazi, N.,](#)
725 [Chevallier, P., Dimri, A.P., Kulkarni, A.V., Cogley, J.G., Bahuguna, I.: Glaciohydrology of the](#)
726 [Himalaya-Karakoram. *Science*, 373: eabf3668, https://doi.org/10.1126/science.abf3668](#), 2021.
727 [Battamo, A.Y., Varis, O., Sun, P., Yang, Y., Oba, B.T., Zhao, L.: Mapping socio-ecological resilience along the](#)
728 [seven economic corridors of the Belt and Road Initiative. *J. Clean. Prod.*, 309: 127341,](#)
729 <https://doi.org/10.1016/j.jclepro.2021.127341>, 2021.
730 [Bhambri, R., Hewitt, K., Kawishwar, P., Kumar, A., Verma, A., Snehmani, Tiwari, S., Misra, A.: Ice-dams,](#)
731 [outburst floods, and movement heterogeneity of glaciers, Karakoram. *Global Planet. Change*, 180: 100-116,](#)
732 <https://doi.org/10.1016/j.gloplacha.2019.05.004>, 2019.

733 [Bhattacharya, A., Bolch, T., Mukherjee, K., King, O., Menounos, B., Kapitsa, V., Neckel, N., Yang, W., Yao, T.:](#)
734 [High Mountain Asian glacier response to climate revealed by multi-temporal satellite observations since the](#)
735 [1960s. Nat. Commun., 12: 4133, <https://doi.org/10.1038/s41467-021-24180-y>, 2021.](#)

736 [Bolch, T., Pieczonka, T., Mukherjee, K., Shea, J.: Brief communication: Glaciers in the Hunza catchment](#)
737 [\(Karakoram\) have been nearly in balance since the 1970s. The Cryosphere, 11: 531-539,](#)
738 <https://doi.org/10.5194/tc-11-531-2017>, 2017.

739 [Brun, F., Berthier, E., Wagnon, P., Kääb, A., Treichler, D.: A spatially resolved estimate of High Mountain Asia](#)
740 [glacier mass balances from 2000 to 2016. Nat. Geosci., 10: 668-673, <https://doi.org/10.1038/ngeo2999>, 2017.](#)

741 [Brun, F., Wagnon, P., Berthier, E., Jomelli, V., Maharjan, S.B., Shrestha, F., Kraaijenbrink, P.D.A.:](#)
742 [Heterogeneous Influence of Glacier Morphology on the Mass Balance Variability in High Mountain Asia. J.](#)
743 [Geophys. Res-Earth, 124: 1331-1345, <https://doi.org/10.1029/2018JF004838>, 2019.](#)

744 [Carrivick, J.L., Tweed, F.S.: Proglacial lakes: character, behaviour and geological importance. Quaternary Sci.](#)
745 [Rev., 78: 34-52, <https://doi.org/10.1016/j.quascirev.2013.07.028>, 2013.](#)

746 [Carrivick, J.L., Quincey, D.J.: Progressive increase in number and volume of ice-marginal lakes on the western](#)
747 [margin of the Greenland Ice Sheet. Global Planet. Change, 116: 156-163,](#)
748 <https://doi.org/10.1016/j.gloplacha.2014.02.009>, 2014.

749 [Carrivick, J.L., Tweed, F.S.: A global assessment of the societal impacts of glacier outburst floods. Global](#)
750 [Planet. Change, 144: 1-16, <https://doi.org/10.1016/j.gloplacha.2016.07.001>, 2016.](#)

751 [Carrivick, J.L., Tweed, F.S., Sutherland, J.L., Mallalieu, J.: Toward Numerical Modeling of Interactions](#)
752 [Between Ice-Marginal Proglacial Lakes and Glaciers. Front. Earth Sci, 8,](#)
753 <https://doi.org/10.3389/feart.2020.577068>, 2020.

754 [Chen, F., Zhang, M., Guo, H., Allen, S., Kargel, J.S., Haritashya, U.K., Watson, C.S.: Annual 30 m dataset for](#)

755 [glacial lakes in High Mountain Asia from 2008 to 2017. Earth System Science Data, 13: 741-766,](#)
756 <https://doi.org/10.5194/essd-13-741-2021>, 2021.

757 [Chen, X., Cui, P., You, Y., Cheng, Z., Khan, A., Ye, C., Zhang, S.: Dam-break risk analysis of the Attabad](#)
758 [landslide dam in Pakistan and emergency countermeasures. Landslides, 14: 675-683,](#)
759 <https://doi.org/10.1007/s10346-016-0721-7>, 2017.

760 [Emmer, A., Cuřín, V.: Can a dam type of an alpine lake be derived from lake geometry? A negative result. J. Mt.](#)
761 [Sci.-Engl., 18: 614-621, https://doi.org/10.1007/s11629-020-6003-9, 2021.](#)

762 [Farr, T.G., Rosen, P.A., Caro, E., Crippen, R., Duren, R., Hensley, S., Kobrick, M., Paller, M., Rodriguez, E.,](#)
763 [Roth, L., Seal, D., Shaffer, S., Shimada, J., Umland, J., Werner, M., Oskin, M., Burbank, D., Alsdorf, D.: The](#)
764 [Shuttle Radar Topography Mission. Rev. Geophys., 45: RG2004, https://doi.org/10.1029/2005RG000183, 2007.](#)

765 [Gardelle, J., Arnaud, Y., Berthier, E.: Contrasted evolution of glacial lakes along the Hindu Kush Himalaya](#)
766 [mountain range between 1990 and 2009. Global Planet. Change, 75: 47-55,](#)
767 <https://doi.org/10.1016/j.gloplacha.2010.10.003>, 2011.

768 [Hanshaw, M.N., Bookhagen, B.: Glacial areas, lake areas, and snow lines from 1975 to 2012: status of the](#)
769 [Cordillera Vilcanota, including the Quelccaya Ice Cap, northern central Andes, Peru. The Cryosphere, 8:](#)
770 [359-376, https://doi.org/10.5194/tc-8-359-2014, 2014.](#)

771 [Hewitt, K.: The Karakoram Anomaly? Glacier Expansion and the 'Elevation Effect,' Karakoram Himalaya. Mt.](#)
772 [Res. Dev., 25: 332-340, https://doi.org/10.1659/0276-4741\(2005\)025\[0332:TKAGEA\]2.0.CO;2, 2005.](#)

773 [Hewitt, K., 2014. Glaciers of the Karakoram Himalaya: Glacial Environments, Processes, Hazards and](#)
774 [Resources. Springer, Dordrecht.](#)

775 [How, P., Messerli, A., Mätzler, E., Santoro, M., Wiesmann, A., Caduff, R., Langley, K., Bojesen, M.H., Paul, F.,](#)
776 [K ääb, A., Carrivick, J.L.: Greenland-wide inventory of ice marginal lakes using a multi-method approach. Sci.](#)

777 [Rep.-UK, 11: 4481, https://doi.org/10.1038/s41598-021-83509-1, 2021.](https://doi.org/10.1038/s41598-021-83509-1)

778 [Huggel, C., Kääb, A., Haerberli, W., Teysseire, P., Paul, F.: Remote sensing based assessment of hazards from](https://doi.org/10.1139/t01-099)

779 [glacier lake outbursts: a case study in the Swiss Alps. Can. Geotech. J., 39: 316-330,](https://doi.org/10.1139/t01-099)

780 [https://doi.org/10.1139/t01-099, 2002.](https://doi.org/10.1139/t01-099)

781 [Hugonnet, R., McNabb, R., Berthier, E., Menounos, B., Nuth, C., Girod, L., Farinotti, D., Huss, M., Dussaillant,](https://doi.org/10.1038/s41586-021-03436-z)

782 [I., Brun, F., Kääb, A.: Accelerated global glacier mass loss in the early twenty-first century. Nature, 592:](https://doi.org/10.1038/s41586-021-03436-z)

783 [726-731, https://doi.org/10.1038/s41586-021-03436-z, 2021.](https://doi.org/10.1038/s41586-021-03436-z)

784 [Jarvis, A., Reuter, H.I., Nelson, A., Guevara, E., 2008. Hole-filled seamless SRTM data V4. 2008, International](http://srtm.csi.cgiar.org)

785 [Centre for Tropical Agriculture \(CIAT\), available from http://srtm.csi.cgiar.org.](http://srtm.csi.cgiar.org)

786 [Jiang, S., Nie, Y., Liu, Q., Wang, J., Liu, L., Hassan, J., Liu, X., Xu, X.: Glacier Change, Supraglacial Debris](https://doi.org/10.3390/rs10070986)

787 [Expansion and Glacial Lake Evolution in the Gyirong River Basin, Central Himalayas, between 1988 and 2015.](https://doi.org/10.3390/rs10070986)

788 [Remote Sens.-Basel, 10: 986, https://doi.org/10.3390/rs10070986, 2018.](https://doi.org/10.3390/rs10070986)

789 [Kääb, A., Berthier, E., Nuth, C., Gardelle, J., Arnaud, Y.: Contrasting patterns of early twenty-first-century](https://doi.org/10.1038/nature11324)

790 [glacier mass change in the Himalayas. Nature, 488: 495-498, https://doi.org/10.1038/nature11324, 2012.](https://doi.org/10.1038/nature11324)

791 [Lesi, M., Nie, Y., Shugar, D.H., Wang, J., Deng, Q., Chen, H.: Landsat and Sentinel-derived glacial lake dataset](https://doi.org/10.12380/Glaci.msdc.000001)

792 [in the China-Pakistan Economic Corridor from 1990 to 2020. Mountain Science Data Center,](https://doi.org/10.12380/Glaci.msdc.000001)

793 [https://doi.org/10.12380/Glaci.msdc.000001 CSTR:1a006.11.Glaci.msdc.000001, 2022.](https://doi.org/10.12380/Glaci.msdc.000001)

794 [Li, D., Shangguan, D., Anjum, M.N.: Glacial Lake Inventory Derived from Landsat 8 OLI in 2016–2018 in](https://doi.org/10.3390/ijgi9050294)

795 [China–Pakistan Economic Corridor. ISPRS international journal of geo-information, 9: 294,](https://doi.org/10.3390/ijgi9050294)

796 [https://doi.org/10.3390/ijgi9050294, 2020.](https://doi.org/10.3390/ijgi9050294)

797 [Li, Z., Deng, X., Zhang, Y.: Evaluation and convergence analysis of socio-economic vulnerability to natural](https://doi.org/10.3390/ijgi9050294)

798 [hazards of Belt and Road Initiative countries. J. Clean. Prod., 282: 125406,](https://doi.org/10.3390/ijgi9050294)

799 <https://doi.org/10.1016/j.jclepro.2020.125406>, 2021.

800 [Liu, Q., Mayer, C.: Distribution and interannual variability of supraglacial lakes on debris-covered glaciers in](#)
801 [the Khan Tengri-Tumor Mountains, Central Asia. Environ. Res. Lett., 10: 014014 2015.](#)

802 [Liu, Q., Mayer, C., Wang, X., Nie, Y., Wu, K., Wei, J., Liu, S.: Interannual flow dynamics driven by frontal](#)
803 [retreat of a lake-terminating glacier in the Chinese Central Himalaya. Earth Planet. Sc. Lett., 546: 116450.](#)
804 <https://doi.org/10.1016/j.epsl.2020.116450>, 2020.

805 [Lutz, A.F., Immerzeel, W.W., Shrestha, A.B., Bierkens, M.F.P.: Consistent increase in High Asia's runoff due to](#)
806 [increasing glacier melt and precipitation. Nat. Clim. Change, 4: 587-592, https://doi.org/10.1038/nclimate2237,](#)
807 [2014.](#)

808 [Lyons, E.A., Sheng, Y., Smith, L.C., Li, J., Hinkel, K.M., Lenters, J.D., Wang, J.: Quantifying sources of error](#)
809 [in multitemporal multisensor lake mapping. Int. J. Remote Sens., 34: 7887-7905,](#)
810 <https://doi.org/10.1080/01431161.2013.827343>, 2013.

811 [Martín, C.N.S., Ponce, J.F., Montes, A., Balocchi, L.D., Gorza, C., Andrea, C.: Proglacial landform assemblage](#)
812 [in a rapidly retreating cirque glacier due to temperature increase since 1970, Fuegian Andes, Argentina.](#)
813 [Geomorphology, 390: 107861, https://doi.org/10.1016/j.geomorph.2021.107861](#), 2021.

814 [Maurer, J.M., Schaefer, J.M., Rupper, S., Corley, A.: Acceleration of ice loss across the Himalayas over the past](#)
815 [40 years. Sci. Adv., 5: eaav7266, https://doi.org/10.1126/sciadv.aav7266](#), 2019.

816 [Mcfeeters, S.K.: The use of the Normalized Difference Water Index \(NDWI\) in the delineation of open water](#)
817 [features. Int. J. Remote Sens., 17: 1425 - 1432 1996.](#)

818 [Miles, E.S., Watson, C.S., Brun, F., Berthier, E., Esteves, M., Quincey, D.J., Miles, K.E., Hubbard, B., Wagon,](#)
819 [P.: Glacial and geomorphic effects of a supraglacial lake drainage and outburst event, Everest region, Nepal](#)
820 [Himalaya. The Cryosphere, 12: 3891-3905, https://doi.org/10.5194/tc-12-3891-2018](#), 2018.

821 [Nie, Y., Zhang, Y., Liu, L., Zhang, J.: Glacial change in the vicinity of Mt. Qomolangma \(Everest\), central high](#)
822 [Himalayas since 1976. J. Geogr. Sci., 20: 667-686, <https://doi.org/10.1007/s11442-010-0803-8>, 2010.](#)

823 [Nie, Y., Sheng, Y., Liu, Q., Liu, L., Liu, S., Zhang, Y., Song, C.: A regional-scale assessment of Himalayan](#)
824 [glacial lake changes using satellite observations from 1990 to 2015. Remote Sens. Environ., 189: 1-13,](#)
825 <https://doi.org/10.1016/j.rse.2016.11.008>, 2017.

826 [Nie, Y., Liu, Q., Wang, J., Zhang, Y., Sheng, Y., Liu, S.: An inventory of historical glacial lake outburst floods](#)
827 [in the Himalayas based on remote sensing observations and geomorphological analysis. Geomorphology, 308:](#)
828 [91-106, <https://doi.org/10.1016/j.geomorph.2018.02.002>, 2018.](https://doi.org/10.1016/j.geomorph.2018.02.002)

829 [Nie, Y., Liu, W., Liu, Q., Hu, X., Westoby, M.J.: Reconstructing the Chongbaxia Tsho glacial lake outburst](#)
830 [flood in the Eastern Himalaya: Evolution, process and impacts. Geomorphology, 370: 107393,](#)
831 <https://doi.org/10.1016/j.geomorph.2020.107393>, 2020.

832 [Nie, Y., Pritchard, H.D., Liu, Q., Hennig, T., Wang, W., Wang, X., Liu, S., Nepal, S., Samyn, D., Hewitt, K.,](#)
833 [Chen, X.: Glacial change and hydrological implications in the Himalaya and Karakoram. Nature Reviews Earth](#)
834 [& Environment, 2: 91-106, <https://doi.org/10.1038/s43017-020-00124-w>, 2021.](#)

835 [Paul, F., Rastner, P., Azzoni, R.S., Diolaiuti, G., Fugazza, D., Le Bris, R., Nemec, J., Rabatel, A., Ramusovic,](#)
836 [M., Schwaizer, G., Smiraglia, C.: Glacier shrinkage in the Alps continues unabated as revealed by a new glacier](#)
837 [inventory from Sentinel-2. Earth System Science Data, 12: 1805-1821,](#)
838 <https://doi.org/10.5194/essd-12-1805-2020>, 2020.

839 [Pfeffer, W.T., Arendt, A.A., Bliss, A., Bolch, T., Cogley, J.G., Gardner, A.S., Hagen, J., Hock, R., Kaser, G.,](#)
840 [Kienholz, C., Miles, E.S., Moholdt, G., Mölg, N., Paul, F., Radić, V., Rastner, P., Raup, B.H., Rich, J., Sharp,](#)
841 [M.J.: The Randolph Glacier Inventory: a globally complete inventory of glaciers. J. Glaciol., 60: 537-552,](#)
842 <https://doi.org/10.3189/2014JoG13J176>, 2014.

843 [Post, A., Mayo, L.R., 1971. Glacier dammed lakes and outburst floods in Alaska: U.S. Geological Survey](#)
844 [Hydrologic Investigations Atlas 455, U.S. Geological Survey.](#)

845 [Pritchard, H.D.: Asia's shrinking glaciers protect large populations from drought stress. Nature, 569: 649-654,](#)
846 <https://doi.org/10.1038/s41586-019-1240-1>, 2019.

847 [Quincey, D.J., Richardson, S.D., Luckman, A., Lucas, R.M., Reynolds, J.M., Hambrey, M.J., Glasser, N.F.:](#)
848 [Early recognition of glacial lake hazards in the Himalaya using remote sensing datasets. Global Planet. Change,](#)
849 [56: 137-152, https://doi.org/10.1016/j.gloplacha.2006.07.013, 2007.](#)

850 [Rabus, B., Eineder, M., Roth, A., Bamler, R.: The shuttle radar topography mission—a new class of digital](#)
851 [elevation models acquired by spaceborne radar. ISPRS J. Photogramm., 57: 241-262,](#)
852 [https://doi.org/10.1016/S0924-2716\(02\)00124-7](https://doi.org/10.1016/S0924-2716(02)00124-7), 2003.

853 [RGI Consortium: Randolph Glacier Inventory – A Dataset of Global Glacier Outlines: Version 6.0: Technical](#)
854 [Report, https://doi.org/10.7265/N5-RGI-60, 2017.](#)

855 [Rick, B., Mcgrath, D., Armstrong, W., Mccoy, S.W.: Dam type and lake location characterize ice-marginal lake](#)
856 [area change in Alaska and NW Canada between 1984 and 2019. The Cryosphere, 16: 297-314,](#)
857 <https://doi.org/10.5194/tc-16-297-2022>, 2022.

858 [Rounce, D.R., Hock, R., Shean, D.E.: Glacier Mass Change in High Mountain Asia Through 2100 Using the](#)
859 [Open-Source Python Glacier Evolution Model \(PyGEM\). Front. Earth Sci, 7: 331,](#)
860 <https://doi.org/10.3389/feart.2019.00331>, 2020.

861 [Roy, D.P., Wulder, M.A., Loveland, T.R., C. E., W., Allen, R.G., Anderson, M.C., Helder, D., Irons, J.R.,](#)
862 [Johnson, D.M., Kennedy, R., Scambos, T.A., Schaaf, C.B., Schott, J.R., Sheng, Y., Vermote, E.F., Belward,](#)
863 [A.S., Bindschadler, R., Cohen, W.B., Gao, F., Hipple, J.D., Hostert, P., Huntington, J., Justice, C.O., Kilic, A.,](#)
864 [Kovalskyy, V., Lee, Z.P., Lymburner, L., Masek, J.G., Mccorkel, J., Shuai, Y., Trezza, R., Vogelmann, J.,](#)

865 [Wynne, R.H., Zhu, Z.: Landsat-8: Science and product vision for terrestrial global change research. Remote](#)
866 [Sens. Environ., 145: 154-172, <https://doi.org/10.1016/j.rse.2014.02.001>, 2014.](#)

867 [Sakai, A.: Brief communication: Updated GAMDAM glacier inventory over high-mountain Asia. The](#)
868 [Cryosphere, 13: 2043-2049, <https://doi.org/10.5194/tc-13-2043-2019>, 2019.](#)

869 [Shean, D.E., Bhushan, S., Montesano, P., Rounce, D.R., Arendt, A., Osmanoglu, B.: A Systematic, Regional](#)
870 [Assessment of High Mountain Asia Glacier Mass Balance. Front. Earth Sci, 7: 363,](#)
871 <https://doi.org/10.3389/feart.2019.00363>, 2020.

872 [Sheng, Y., Song, C., Wang, J., Lyons, E.A., Knox, B.R., Cox, J.S., Gao, F.: Representative lake water extent](#)
873 [mapping at continental scales using multi-temporal Landsat-8 imagery. Remote Sens. Environ., 185: 129-141,](#)
874 <https://doi.org/10.1016/j.rse.2015.12.041>, 2016.

875 [Shugar, D.H., Burr, A., Haritashya, U.K., Kargel, J.S., Watson, C.S., Kennedy, M.C., Bevington, A.R., Betts,](#)
876 [R.A., Harrison, S., Stratman, K.: Rapid worldwide growth of glacial lakes since 1990. Nat. Clim. Change, 10:](#)
877 [939-945, <https://doi.org/10.1038/s41558-020-0855-4>, 2020.](#)

878 [Shugar, D.H., Jacquemart, M., Shean, D., Bhushan, S., Upadhyay, K., Sattar, A., Schwanghart, W., McBride, S.,](#)
879 [de Vries, M., Mergili, M., Emmer, A., Deschamps-Berger, C., McDonnell, M., Bhambri, R., Allen, S., Berthier,](#)
880 [E., Carrivick, J.L., Clague, J.J., Dokukin, M., Dunning, S.A., Frey, H., Gascoin, S., Haritashya, U.K., Huggel,](#)
881 [C., Kaab, A., Kargel, J.S., Kavanaugh, J.L., Lacroix, P., Petley, D., Rupper, S., Azam, M.F., Cook, S.J., Dimri,](#)
882 [A.P., Eriksson, M., Farinotti, D., Fiddes, J., Gnyawali, K.R., Harrison, S., Jha, M., Koppes, M., Kumar, A.,](#)
883 [Leinss, S., Majeed, U., Mal, S., Muhuri, A., Noetzli, J., Paul, F., Rashid, I., Sain, K., Steiner, J., Ugalde, F.,](#)
884 [Watson, C.S., Westoby, M.J.: A massive rock and ice avalanche caused the 2021 disaster at Chamoli, Indian](#)
885 [Himalaya. Science, 373: 300-306, <https://doi.org/10.1126/science.abh4455>, 2021.](#)

886 [Ullah, S., You, Q., Ali, A., Ullah, W., Jan, M.A., Zhang, Y., Xie, W., Xie, X.: Observed changes in maximum](#)

887 [and minimum temperatures over China- Pakistan economic corridor during 1980–2016. Atmos. Res., 216:](#)
888 [37-51, https://doi.org/10.1016/j.atmosres.2018.09.020, 2019.](#)

889 [Viviroli, D., Kummu, M., Meybeck, M., Kallio, M., Wada, Y.: Increasing dependence of lowland populations](#)
890 [on mountain water resources. Nature Sustainability, 3: 917-928, https://doi.org/10.1038/s41893-020-0559-9,](#)
891 [2020.](#)

892 [Wang, J., Sheng, Y., Tong, T.S.D.: Monitoring decadal lake dynamics across the Yangtze Basin downstream of](#)
893 [Three Gorges Dam. Remote Sens. Environ., 152: 251-269, https://doi.org/10.1016/j.rse.2014.06.004, 2014.](#)

894 [Wang, J., Sheng, Y., Wada, Y.: Little impact of the Three Gorges Dam on recent decadal lake decline across](#)
895 [China's Yangtze Plain. Water Resour. Res., 53: 3854-3877, https://doi.org/10.1002/2016WR019817, 2017.](#)

896 [Wang, J., Song, C., Reager, J.T., Yao, F., Famiglietti, J.S., Sheng, Y., Macdonald, G.M., Brun, F., Schmied,](#)
897 [H.M., Marston, R.A., Wada, Y.: Recent global decline in endorheic basin water storages. Nat. Geosci., 11:](#)
898 [926-932, https://doi.org/10.1038/s41561-018-0265-7, 2018.](#)

899 [Wang, X., Ding, Y., Liu, S., Jiang, L., Wu, K., Jiang, Z., Guo, W.: Changes of glacial lakes and implications in](#)
900 [Tian Shan, Central Asia, based on remote sensing data from 1990 to 2010. Environ. Res. Lett., 8: 44052,](#)
901 [https://doi.org/10.1088/1748-9326/8/4/044052, 2013.](#)

902 [Wang, X., Liu, S., Zhang, J.: A new look at roles of the cryosphere in sustainable development. Advances in](#)
903 [Climate Change Research, 10: 124-131, https://doi.org/10.1016/j.accre.2019.06.005, 2019.](#)

904 [Wang, X., Guo, X., Yang, C., Liu, Q., Wei, J., Zhang, Y., Liu, S., Zhang, Y., Jiang, Z., Tang, Z.: Glacial lake](#)
905 [inventory of high-mountain Asia in 1990 and 2018 derived from Landsat images. Earth System Science Data,](#)
906 [12: 2169-2182, https://doi.org/10.5194/essd-12-2169-2020, 2020.](#)

907 [Wangchuk, S., Bolch, T.: Mapping of glacial lakes using Sentinel-1 and Sentinel-2 data and a random forest](#)
908 [classifier: Strengths and challenges. Science of Remote Sensing, 2: 100008,](#)

909 <https://doi.org/https://doi.org/10.1016/j.srs.2020.100008>, 2020.

910 [Westoby, M.J., Glasser, N.F., Brasington, J., Hambrey, M.J., Quincey, D.J., Reynolds, J.M.: Modelling outburst](#)

911 [floods from moraine-dammed glacial lakes. Earth-Sci. Rev., 134: 137-159,](#)

912 <https://doi.org/10.1016/j.earscirev.2014.03.009>, 2014.

913 [Williamson, A.G., Banwell, A.F., Willis, I.C., Arnold, N.S.: Dual-satellite \(Sentinel-2 and Landsat 8\) remote](#)

914 [sensing of supraglacial lakes in Greenland. The Cryosphere, 12: 3045-3065,](#)

915 <https://doi.org/10.5194/tc-12-3045-2018>, 2018.

916 [Wulder, M.A., Loveland, T.R., Roy, D.P., Crawford, C.J., Masek, J.G., Woodcock, C.E., Allen, R.G., Anderson,](#)

917 [M.C., Belward, A.S., Cohen, W.B., Dwyer, J., Erb, A., Gao, F., Griffiths, P., Helder, D., Hermosilla, T., Hipple,](#)

918 [J.D., Hostert, P., Hughes, M.J., Huntington, J., Johnson, D.M., Kennedy, R., Kilic, A., Li, Z., Lymburner, L.,](#)

919 [McCorkel, J., Pahlevan, N., Scambos, T.A., Schaaf, C., Schott, J.R., Sheng, Y., Storey, J., Vermote, E.,](#)

920 [Vogelmann, J., White, J.C., Wynne, R.H., Zhu, Z.: Current status of Landsat program, science, and applications.](#)

921 [Remote Sens. Environ., 225: 127-147, https://doi.org/https://doi.org/10.1016/j.rse.2019.02.015](#), 2019.

922 [Yao, C., Wang, X., Zhao, X., Wei, J., Zhang, Y.: Temporal and Spatial Changes of Glacial Lakes in the](#)

923 [China-Pakistan Economic Corridor from 1990 to 2018. Journal of Glaciology and Geocryology, 42: 33-42,](#)

924 <https://doi.org/https://doi.org/10.7522/j.issn.1000-0240.2020.0009>, 2020.

925 [Yao, T., Thompson, L., Yang, W., Yu, W.S., Gao, Y., Guo, X.J., Yang, X.X., Duan, K.Q., Zhao, H.B., Xu, B.Q.,](#)

926 [Pu, J.C., Lu, A.X., Xiang, Y., Kattel, D.B., Joswiak, D.: Different glacier status with atmospheric circulations in](#)

927 [Tibetan Plateau and surroundings. Nat. Clim. Change, 2: 663-667, https://doi.org/10.1038/NCLIMATE1580,](#)

928 [2012.](#)

929 [Yao, X., Liu, S., Han, L., Sun, M., Zhao, L.: Definition and classification system of glacial lake for inventory](#)

930 [and hazards study. J. Geogr. Sci., 28: 193-205, https://doi.org/10.1007/s11442-018-1467-z](#), 2018.

931 [Zhang, G., Yao, T., Xie, H., Wang, W., Yang, W.: An inventory of glacial lakes in the Third Pole region and](#)
932 [their changes in response to global warming. Global Planet. Change, 131: 148-157,](#)
933 <https://doi.org/10.1016/j.gloplacha.2015.05.013>, 2015.

934 [Zhang, M., Chen, F., Tian, B.: An automated method for glacial lake mapping in High Mountain Asia using](#)
935 [Landsat 8 imagery. J. Mt. Sci.-Engl., 15: 13-24, https://doi.org/10.1007/s11629-017-4518-5](#), 2018.

936 [Zhao, W., Xiong, D., Wen, F., Wang, X.: Lake area monitoring based on land surface temperature in the Tibetan](#)
937 [Plateau from 2000 to 2018. Environ. Res. Lett., 15, https://doi.org/10.1088/1748-9326/ab9b41](#), 2020.

938 [Zheng, G., Allen, S.K., Bao, A., Ballesteros-C ánovas, J.A., Huss, M., Zhang, G., Li, J., Yuan, Y., Jiang, L., Yu,](#)
939 [T., Chen, W., Stoffel, M.: Increasing risk of glacial lake outburst floods from future Third Pole deglaciation. Nat.](#)
940 [Clim. Change, 11: 411-417, https://doi.org/10.1038/s41558-021-01028-3](#), 2021.

941 _____
942 _____

943 [Appendix](#)
944 [Tutorial for Improved Uncertainty Estimating Method](#)

945
946 [The Hanshaw’s equation was originally proposed for pixelated polygons \(such as a polygon directly](#)
947 [extracted from a remote sensing image\), and performed more robustly than manually digitized polygons](#)
948 [\(where vertices do not necessarily follow the pixel edges\). Our improved method also performs better for](#)
949 [pixelated polygons. This tutorial is dedicated to helping implement our improved uncertainty estimation](#)
950 [method.](#)

951
952 [Procedure of uncertainty estimating method \(using ArcGIS for example\)](#)

953 [1. Removing redundant nodes \(optional\)](#)

954 [We found that a small proportion \(~1%\) of the pixelated lake polygons \(directly extracted from satellite](#)
955 [images\) have redundant nodes, which affects the value of inner nodes. If no redundant nodes exist, this](#)
956 [step can be skipped. Or, we recommend using the “Simplify Polygon” tool in ArcGIS to remove those](#)
957 [nodes \(Figure A1|Figure S1\).](#)

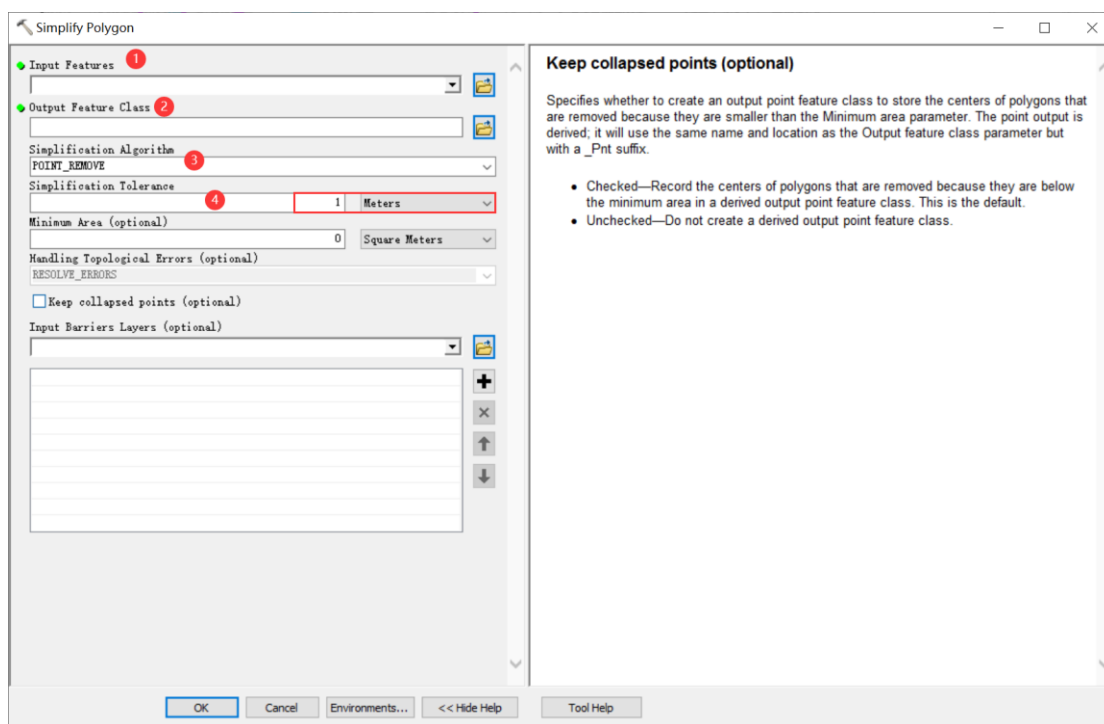
958 [In the Simplify Polygon panel](#)

959 [Input your dataset.](#)

960 [Set the output path and output file name.](#)

961 [Choose the simplification algorithm. We recommended “POINT_REMOVE”.](#)

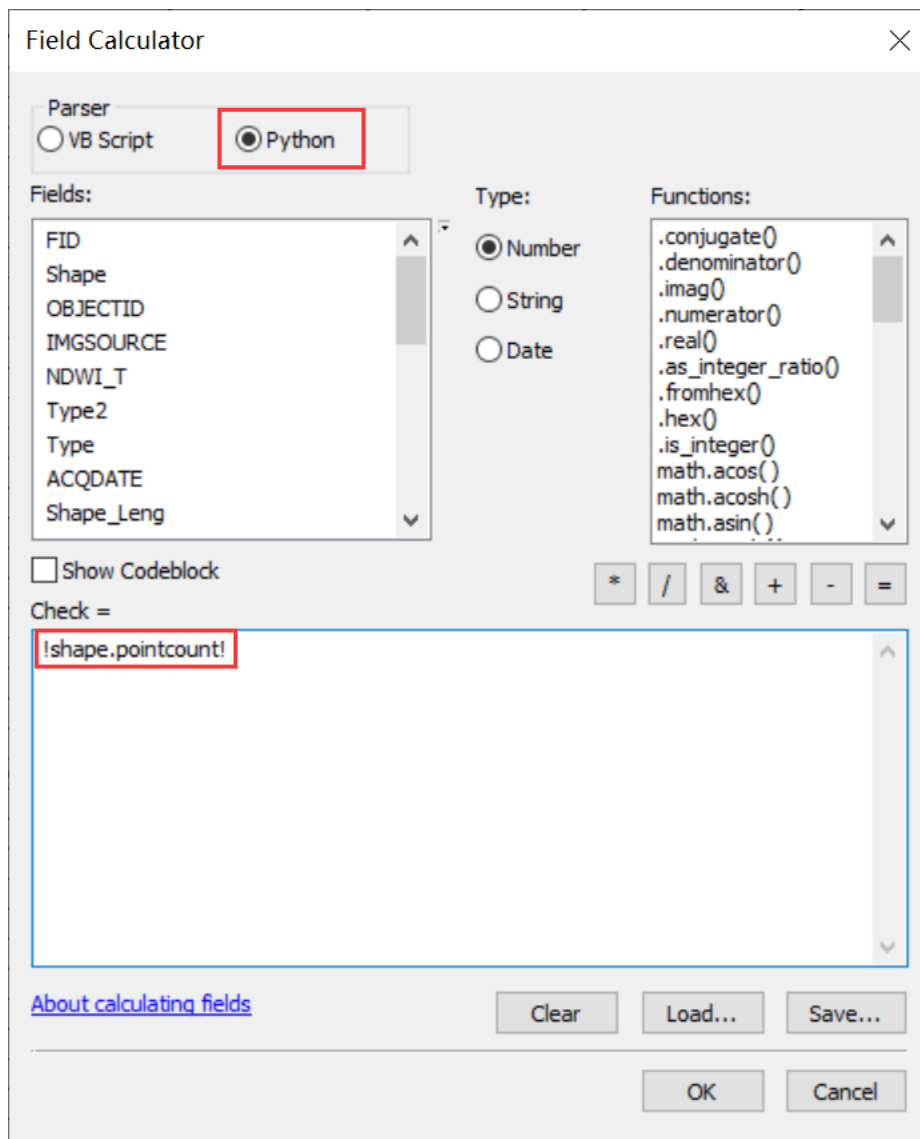
962 [Set the tolerance of simplification algorithm. In this step, we need to ensure that the polygon](#)
963 [boundaries remain unchanged after deleting redundant nodes. Generally, a tolerance of 1 meter will suffice,](#)
964 [or you can adjust the threshold until your satisfaction.](#)



965
966 [Figure A1. Input and option for Simplify Polygon in ArcGIS.](#)~~Figure S1. Input and option for Simplify~~
967 [Polygon in ArcGIS.](#)

968
969 [2. Calculating the total number of nodes using ArcGIS \(Figure A|Figure S22\):](#)

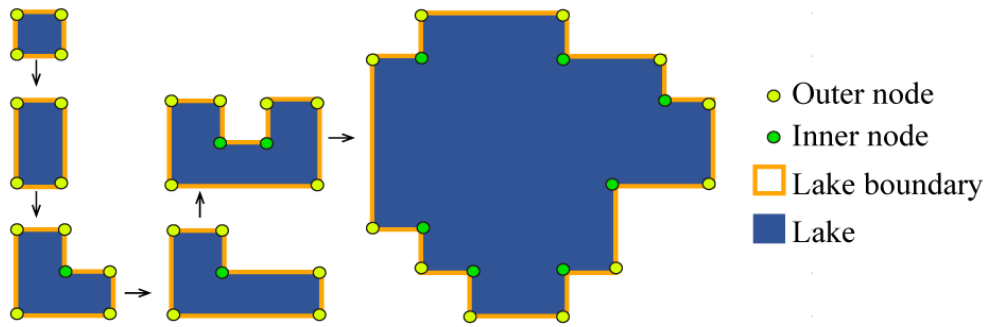
- 970 [Add a new field in the attribute table of dataset.](#)
- 971 [Open Field Calculator.](#)
- 972 [Switch the parser to python mode, and enter the following code “!shape.pointcount!” in the blue box](#)
- 973 [to calculate the total number of nodes for each glacial lake boundary.](#)



974
975 [Figure SA22. Total node calculation in ArcGIS.](#)

976
977 [3. Calculating the number of inner nodes:](#)

978
979 [For polygons without islands \(Figure AFigure S33\), use the equation 5. An inner node is a polygon vertex](#)
 980 [where the interior angle surrounding it is greater than 180 degrees. An outer node is the opposite of the](#)
 981 [inner node, where the interior angle is less than 180 degrees. We found that the outer nodes are usually four](#)
 982 [more than the inner nodes in our glacial lake dataset. The total nodes in ArcGIS contain one overlapping](#)
 983 [node to close the polygon, meaning the endpoint is also the startpoint. This extra count was deleted in the](#)
 984 [calculation \(equation 5\).](#)



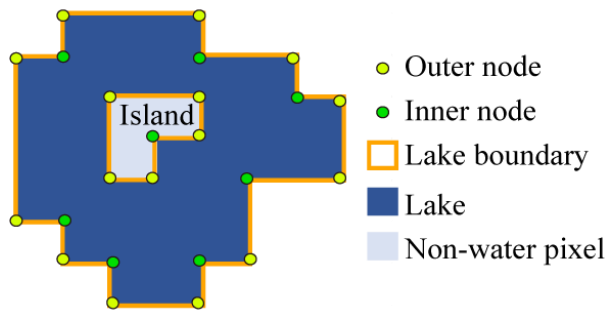
986

987 [Figure SA33](#). Sketch of outer and inner nodes of various glacial lakes without island.

988

989 For polygons with island ([Figure AFigure S44](#)) use the equation 6.

990



991

992 [Figure S4A4](#). Sketch of outer and inner nodes for glacial lake with island.

993

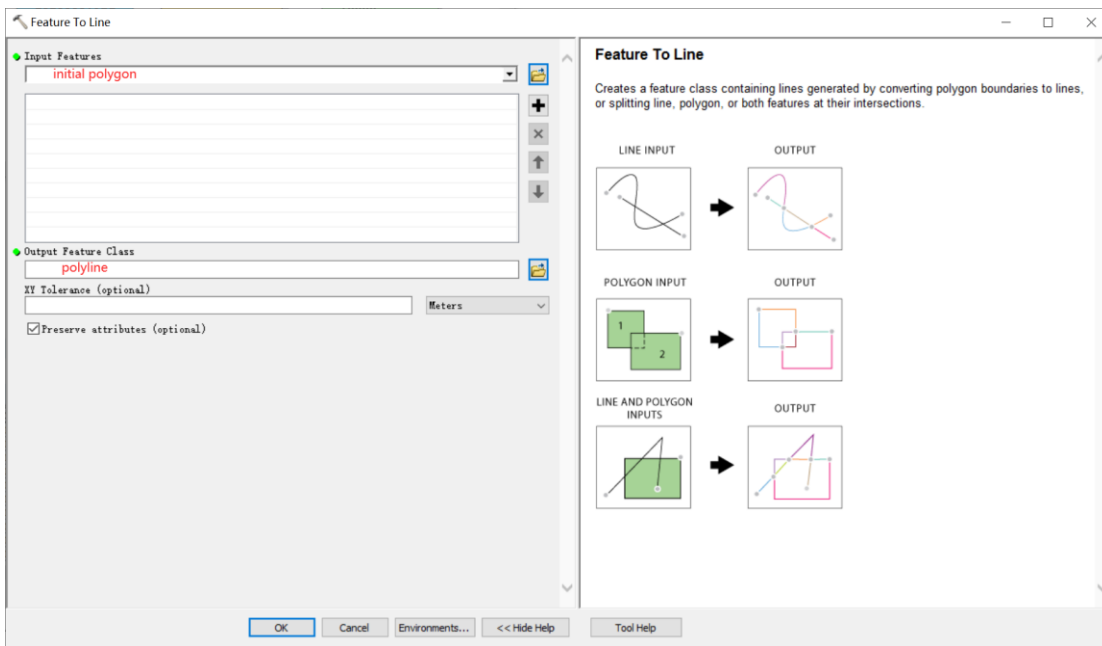
994 We further specify the steps below to help implement equation 6.

995

996 Sept 1: detect the number of islands within each polygon.

997

Convert the initial lake polygon to polyline using the “Feature To Line” tool ([Figure AFigure S55](#)).



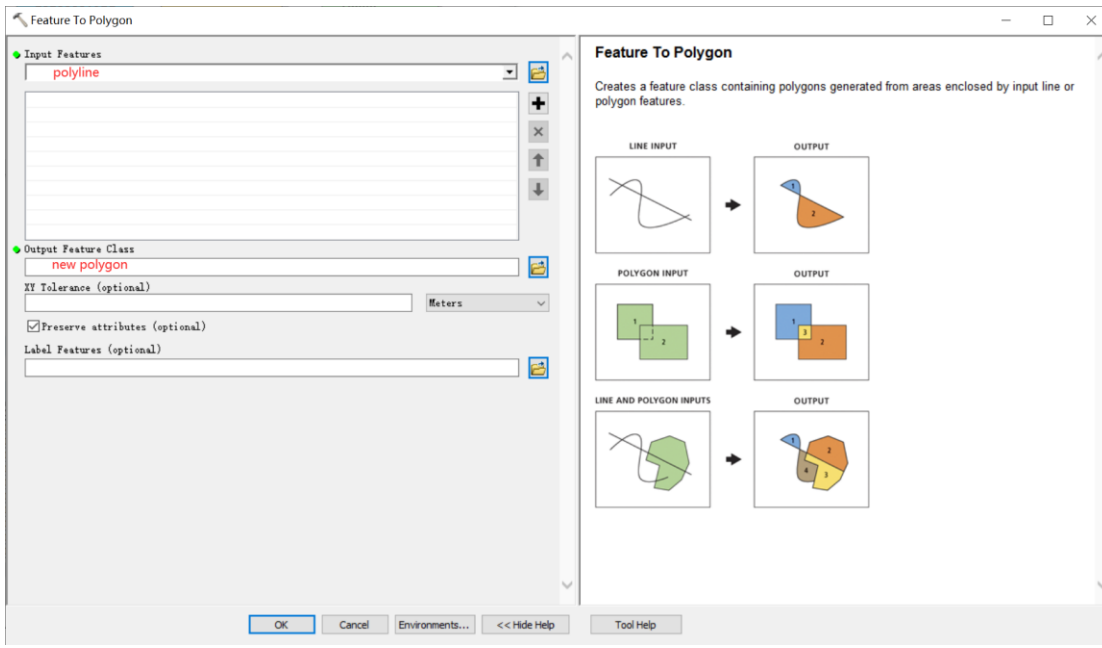
998

999 [Figure SA55](#). Feature To Line tool in ArcGIS

1000

1001

[Convert the polyline to generate a new polygon \(Figure AFigure S66\).](#)



1002

[Figure SA66. Feature To Polygon tool in ArcGIS](#)

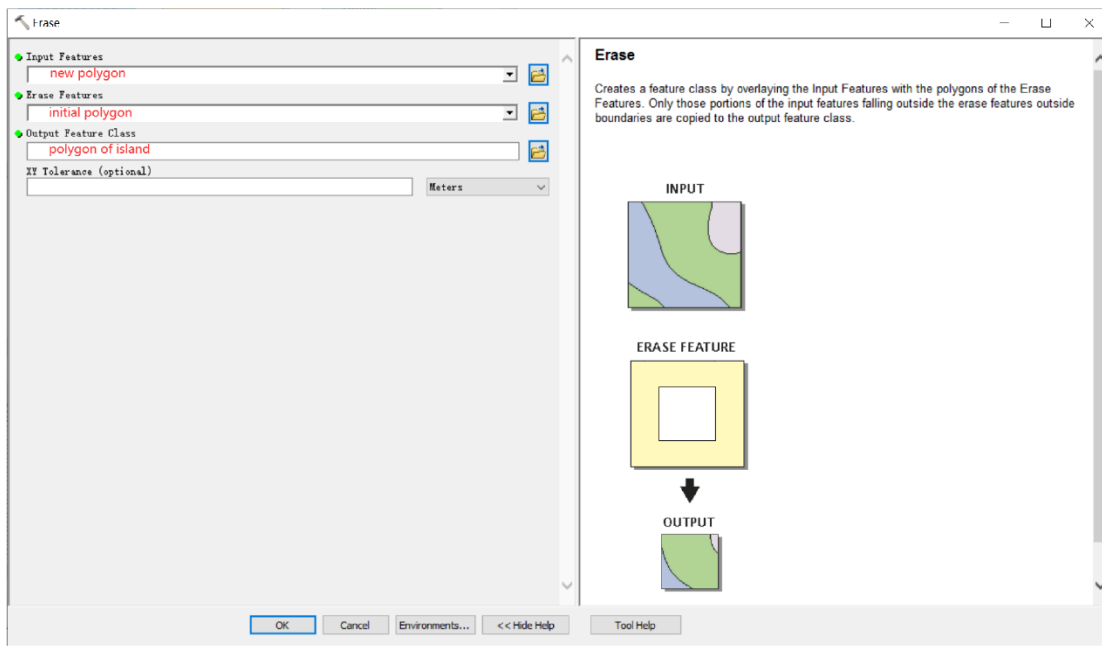
1003

1004

1005

[Erase the new polygon by the initial polygon, which outputs the islands. Then we can count how many islands there are in each lake \(Figure AFigure S77\).](#)

1006



1007

[Figure SA77. Erase tool in ArcGIS.](#)

1008

1009

1010

[Step 2: calculate the number of inner nodes for each polygon with island using equation 6.](#)

1011

1012

[4. Calculating the uncertainty of lake mapping using equation 4.](#)

1013

1014